ADDIS ABABA UNIVERSITY

SCHOOL OF MECHANICAL & INDUSTRIAL ENGINEERING

Performance Analysis of Acetal Nano-Silica composite spur gear

A Thesis submitted to the school of Mechanical & Industrial Engineering of Addis Ababa University in partial fulfillment of the Degree of Masters of Science

In

Mechanical Engineering (Mechanical Design Stream)

By: Bruck Alemu

Advisor: Dr. Daniel Tilahun

Co. Advisor: Ato. Mulugeta H/Mariam

November, 2016

ADDIS ABABA UNIVERSITY

ADDIS ABABA INSTITUTE OF TECHNOLOGY

SCHOOL OF MECHANICAL AND INDUSTRIAL ENGINEERING

Performance Analysis of Acetal Nano-Silica composite spur gear

By: Bruck Alemu

Approved by board of examiners

Mr. Getasew Taddese	_____	_____
Chairman of the school	Signature	Date
Dr. Daniel Tilahun	_____	_____
Advisor	Signature	Date
Ato. Mulugeta H/Mariam	_____	_____
Co. Advisor	Signature	Date
Ato.Tolosa D.	_____	_____
Internal Examiner	Signature	Date
Dr. Tamrat T.	_____	_____
External Examiner	Signature	Date

Declaration

I the undersigned, declare that this thesis entitled `` **Performance Analysis of Acetal nano-silica composite spur gear using FEM''** is the result of my own research carried out under the supervision of Dr. Daniel Tilahun and Ato Mulugeta. It has not been presented in any from in any other university and all sources of material used for this thesis are accordingly sited and acknowledged.

_____ _____

Bruck Alemu Metekia Date

This is to certify that the above declaration made by the candidate is correct to the best of my knowledge.

_____ _____

Dr. Daniel Tilahun Date

Acknowledgment

This research was conducted as a requirement for the fulfillment of my MSc. Degree in mechanical engineering design stream and I would like to thank first Addis Ababa Institute of technology School of mechanical and Industrial Engineering for giving me the opportunity and the fund for my research. I would also like to thank my Advisors Dr. Daniel Tilahun and Ato Mulugeta for their valuable advice and encouragement. I would also like to thank all the staff members of SMIE, and my friends and my family specially my wife and my brother for there all around advise and support. And finally I would like to thank God without whom nothing would have been possible.

Abstract

It is well known that gears are one of the most important and common machine components, and un alternative, light weight and durable, material for gears has been the focus of many researchers, especially in the last two decades. This thesis work will focus on assessing the capability of polymer composite spur gear, acetal, which is the most commonly used polymer for gear manufacturing due to its manufacturability, low cost, and good wear resistance, reinforced with nano-silica (spherical), one of the most easily available and widely used nano particle to reinforce thermoplastics, for medium power transmission(890W). Reinforcing polymers with nano-particles is found to be one of the most effective methods to improve the overall mechanical and thermal property of polymers. The composite gear performance is analyzed for wear and thermal resistance as well as fatigue life. The analysis is conducted with the aid of FEM software Abaqus/CAE 6.14 and the homogenized material property of the composite is predicted using the multi scale homogenization technique which was found to be reliable for calculating the homogenized mechanical property of polymer nano-composites. The results obtained after this work show that the addition of 4.5 volume percentage of nano-silica (SiO_2) in to the polymer matrix (acetal) was found to increase the wear resistance by 300%, the thermal conductivity by 47% and the number of cycles to fatigue failure was found to be ten times more than pure acetal gear, where the change or increase in mass of the gear is only 15.86 grams.

Key words: nano-composite, spur gear, wear resistance, thermal resistance, fatigue life, FEM analysis

Table of Contents

List of Figures

Chapter Two

Chapter Three

Chapter Four

List of Tables

Chapter Two

Chapter Four

Nomenclature

PNC	Polymer nano-composite
G_j^{nan}.	Shear Modulus of the nano-inclusion
K_j^{nan}.	Bulk Modulus of the nano-inclusion
$E_k^{(j).}$	Elastic Modulus of the inter- phase
D_j.	Diameter of the nano-particle
$C_k^{(j)}$.	Volume fraction of the phases
C_{nano}.	Total volume fraction of the Nano size filler
C_{intphs}	Total volume fraction of their interphases
C_{micro} .	Total volume fraction of the microscale fillers
$\Psi(D)$.	Size distribution function
$\psi(D)$.	Density distribution function
$\overline{K}$.	Bulk Modulus of the composite
$\bar{G}$.	Shear Modulus of the composite
REV.	Representative volume element
K_c.	Thermal conductivity of the composite
K_m.	Thermal conductivity of the matrix
K_p.	Thermal conductivity of the particle
ρ_c.	Density of the composite
P_n.	Base pitch
Z_2.	Number of teeth of the driven gear
θ	Pressure angle
θ_f.	Working pressure angle.
a_2.	Addendum coefficient

Chapter One

1 Introduction

1.1 Background

In today's world where, resources are becoming scares, the study and application of alternative materials for different engineering application are of higher interest. As the awareness around engineering polymers grows, there has been a growing application of polymers and polymeric composites for machine parts, which is mainly due to their desirable property. The ability to economically manufacture, there light weight and their ability to run with-out lubrication at increasing temperatures, is making their application more desirable. [1]

A number of works has been published in relation to the performance of polymer gear pair. Polymer gears offer huge potential for high-technology applications and unique advantages over metal gears: low cost, low weight, high efficiency, quietness of operation, functioning without external lubrication, etc. [2]

Polymer and polymer nanocomposite gears are now considered for applications from low-power, precision motion to high power transmission, even in such challenging environments as healthcare and automotive engineering. For example, there are reports in automotive engineering of a 70%reduction in mass, 80% reduction in inertia and up to 9% reduction in fuel consumption by using polymer gears instead of metal. However the application of polymer gears remains limited due to the luck of performance information and design standards. [3]

It is a well-known fact that polymer or plastic gears have inferior mechanical and thermal properties as compared to conventional gear materials, such as steel or brass. They have lower operating temperature, lower manufacturing tolerance and water absorption. There is wide verity of polymers, that can be used for a specific function or application. [4]However, due to the large number of different polymers available, it is very difficult to determine the optimal material combination for a specific gear drive, especially when also considering noise and vibration properties.

Polymer nanocomposite (PNC) materials are new emerging materials which uses the nano sized particle or platelets as reinforcement. The nano-size particle has large specific surface areas and has good interfacial adhesion with compatible polymer. The molecular level interaction between

the nano-size reinforcement and polymer significantly improves the many of their mechanical properties, especially stiffness and strength. Nano-size reinforcement increases the crystallinity of the polymer and reduces the polymeric chain mobility. Nano-size reinforcement also increases the glass transition temperature and barrier properties of the polymer. [5]

In spite of outstanding properties, the polymer composite materials are not finally investigated, and there are still staying some of old but very important aspects which need our further researches. There are required improvements of tribological properties of materials, which lead to life prolongation of polymeric materials and critical details and as the result increase reliability of constructions. And one of the most perspective methods is to fill it by nanoparticles. [6]

1.2 Purpose

As it is indicated in the above paragraphs, it can be seen that even though there are a number of design standards and a number of researches and experiments conduct for the application polymer gears, there still exists a clear gap in the identification of a practical design approach besides the obvious advantages of using polymers as a gear material. So in order to fully exploit the economical, health, (low noise, running without lubrication) and mechanical advantages polymers for gear application further research and experiments are required.

Polymer nanocomposites and their application have become a huge area of interest for researchers due to the mechanical and thermal property enhancement archived by reinforcing polymers with nano particles. But the response of PNC for different engineering application is still not well known and needs more research.

In this paper efforts will be carried out to model a PNC (acetal reinforced with nanosilica) by using the current modeling approach and the possible application of this material as a transmission gear will be assessed by using modeling and simulation software's MATLAB and Abacus/CAE 6.14.

1.3 Literature review

In this section different literatures (articles) are reviewed that are found to be relevant for this thesis work so as to lay the foundation and to get the necessary input for the work to be done in the coming chapters.

1.3.1 Polymer nanocomposites

The development of new materials based on PNCs has been a fast-growing field of research over the last decade. [7] Injection-molded thermoplastic composites have been increasingly used for numerous tribological purposes such as seals, gears and bearings, providing light weight alternatives to metallic components. [8] The large surface area at a rather low Nano filler concentration is one of the attractive features of nanoparticles, because it creates a large inter-phase and interfacial interactions in nanocomposites which introduces various unexpected behavior. The incorporation of inorganic Nano fillers into polymer matrixes has been an effective technique to improve the toughness, stiffness, damping, chemical resistance, heat resistance and coefficient of thermal expansion. [9]

An important aspect of these nanocomposites is that property improvements are attained at very low reinforcement loadings (typically $\leq$ 5wt. %), and strongly depend on the properties of the resin and filler and the compatibility between them, the filler shape, size, surface morphology and concentration, dispersion and distribution of the filler. Consequently, there are differences in reinforcing mechanisms among various particulate-filled polymer composites. [10, 11] In general, the stiffness of nanocomposites tends to increase as the filler volume fraction increases but this relationship is strongly nonlinear. Moreover, there may exist a critical volume fraction beyond which the stiffness starts to decrease. [12]

For applications taking place in hard working conditions, such as slide bearings, the development of composite materials, which possess a high stiffness, toughness and wear resistance, becomes crucial. On the one hand, the extent of the reinforcing effect depends on the properties of composite components, and on the other hand it is strongly affected by the microstructure represented by the filler size, shape, homogeneity of distribution/dispersion of the particles within the polymer, and filler/matrix interface extension. This latter plays a critical role, since the composite material

derives from a combination of properties, which cannot be achieved by either of the components alone. [13]

The study of nanoparticles matrix interface constitutes an important aspect of structural characterization because it underscores the role of the interaction zone in understanding deformation and fracture at the molecular level. [14] It is widely accepted that an interphase exists between the nano fillers and the matrix material. This interphase is a transition region (part of the matrix), over which the mechanical and physical properties change from the properties of filler to the properties of the matrix. This intermediate area extends from nanometers to micrometers. The interphase is usually represented as a third phase around the nanoparticles. [15] Therefore, the polymer–nano filler interface/interphase in nanocomposites is a challengeable matter and many researchers have tried to characterize the interface/interphase characteristics by experimental and theoretical methods with varying degree of success. [16]

An advantage of using nanoparticles compare to macro or micro-fillers as reinforcement is that their size is smaller than the critical crack length that typically initiates failures in composites. Nanoparticles can act as voids and provide improved toughness and strength to the composites. They can also significantly affect glass transition temperature. Typically, this occurs because nanoparticles influence the mobility of the polymer chains due to bonding between the nanoparticles and the polymer and bridging of the polymer chains between the nanoparticles. Higher the interaction between matrix and nanoparticles, more it affects glass transition temperature, as it will increase. [6]

Compared to conventional micron-sized particles, nanoparticles have a much higher surface-to-volume ratio. As the particle size decreases, the percentage of molecules/atoms present on the surface is tremendously increased. As a result, antiparticle forces such as van der Waals and electrostatic forces, as well as magnetic attraction, become stronger. Without proper chemical treatment to reduce the surface energy, it is very common for nanoparticles to form clusters or agglomerates, which are challenging to disperse individually and uniformly in the polymer matrix, thus resulting in opaque nanocomposites akin to conventional composites. [17]

The processing of polymer nanocomposites is generally difficult. There are problems with the agglomeration of nanoparticles and dispersing agents are often needed. Clay nanoparticles need

modification to enable intercalation or exfoliation of the particles. Coupling agents are frequently used to promote bonding of the polymer to the particles. Thus the development of polymer nanocomposites has largely been the province of chemists and the physical characterization of the nanocomposites, such as wide angle X-ray scattering (WAXS) to determine silicate interlayer distances, has generally received more thought than mechanical characterization. In the case of the simpler mechanical properties such as Young's modulus or yield strength the testing techniques are simple and require little thought or interpretation. However, toughness is a more difficult property to characterize. [18]

As it is mentioned on the above paragraphs different researches have been conducted on the area of polymer nanocomposites and all agree that the addition of nano particle in to a polymer matrix will significantly increase the mechanical and thermal property of the polymer. Even though this fact is undisputed the effectiveness of this reinforcing technique depends on many factors mainly on volume fraction and dispersion of the filler as well as the interaction between the matrix and the nano particle. So proper care must be taken during manufacturing of this composites to obtain the optimum material for the required purpose.

1.3.2 The effect of particle size on polymer nanocomposites

Recently Chen et al examined the influence of particle size on damage dissipation in nanocomposites. They applied the concepts of micromechanics and extended it to the de-bonding process of nano-particles, which are characterized by a diameter distribution function. This can only be done as long as the de-bonding process remains relevant over the different lengths scales of the particle size. They concluded on the basis of an energy de-bonding criterion that damage dissipation is strongly dependent on the size of particles and that smaller particles are favorable to increase material toughness. [11]

Cho et al, conducted a systematic experimental and numerical study to address the effect of particle size on elastic modulus, tensile strength and particle/matrix de-bonding fracture toughness of particulate composites. They varied the size of particles from macro (0.5 mm) to nano (15 nm) scale and found that particle size at micro scale impart no influence on Young's modulus of the composite. However, the Young's modulus increased as the size of the particles decreased at nano-scale. [16]

Similar results were obtained by Chisholm et al who infused micro and nano sized Sic particles in epoxy matrix. They claimed that higher elastic modulus in nanocomposites was attained due to higher surface energy of nanoparticles. [19]

According to the literatures mentioned here and other researches is believed that the size of the nano particle will greatly impact the reinforcement of the matrix. As it is mentioned nano sized particles are favorable to increase both the toughness and also the strength of the soft matrix material mainly due to their high surface area to volume ratio, which leads to better interaction with the matrix.

1.3.3 General description of reinforcing theories

Nanocomposites need sufficient stiffness, strength and toughness for their particular design purpose. Stiffness is improved by high modulus particles of any size or shape, though there may be secondary stiffening effects in semi crystalline polymers from the effect of the particles on the lamellar crystal growth. [18]

In general, rigid particles include two kinds: rigid organic particles and rigid inorganic particles. The reinforcing mechanisms and increasing rigidity mechanisms of both rigid organic particles and rigid in organic particles are similar. The inorganic particles used usually as filler in polymer industry have sphere particles, sheet (block) particles, needle (column) particles, etc. In general, there are somewhat differences in reinforcing mechanisms for filled polymer composites among these fillers. [20]

Several reinforcing theories of particulate-filled polymer composites may be concluded as follows: (1) interfacial adhesion reinforcing theory; (2) filler inducing crystallization reinforcing theory; (3) filler frame reinforcing theory; and (4) synergistic reinforcing effect theory. [21]

1.3.3.1 Interfacial adhesion reinforcing theory

When polymer composite is bearing load, the stresses taken by the matrix and filler are transferred through the interface between them, especially for the particulate filled polymer composites. Therefore, interfacial adhesion reinforcing theory believes that the reinforcement of the particulate filled polymer composites depends upon the increase of the interfacial adhesion strength. In other words, the higher the interfacial adhesion strength, the better is the reinforcing effect of the

polymer composites. Under the same interfacial adhesion strength, the larger the interfacial area of the fillers, the better is the reinforcing effect of the polymer composites. [22, 20]

1.3.3.2 Filler inducing crystallization reinforcing theory

It was found in experiments that inorganic filler added to the polymer will play a heterogeneous nucleation. Therefore, the crystallization properties of crystalline polymer will be changed after it is filled with inorganic particles. For example, the super cooled degree of particulate-filled polymer composites will increase with an increase of inorganic particles, but it is lower than that of unfilled resin, this indicates that the adding of inorganic particles will make the filled polymer to be easy crystallization. This may be explained as follows: on the one hand, the interaction between inorganic particles and polymer molecular chains restricts the macromolecules movement, the molecular chains participated in the crystallization decrease relevantly, leading to reduction of the crystallinity of the composites; on the other hand, inorganic particles as a nucleating agent may improve the crystal structure of the polymer, resulting in increase of the crystallinity of the composites. [20]

1.3.3.3 Filler frame reinforcing theory

The theory of filler frame reinforcing and increasing rigidity in particulate filled polymer composites is similar to the theory of filler frame reinforcing and increasing rigidity of the sandstone in concrete. In general, the modulus of inorganic particles is higher or much higher than that of resins. When polymer is filled with inorganic particles, the fillers will limit, to a certain extent, the movement of macromolecular chains, leading to increase of deformation difficulty of the composite systems. When the composite materials are under loading, the stresses are shared and transferred by the matrix and filler, resulting in enhancing obviously the strength and rigidity of polymer composites. In other words, inorganic particles in the matrix play the role of cytoskeleton. [20]

1.3.3.4 Synergistic reinforcing effect theory

The factors affecting the reinforcing mechanisms of the particulate-filled polymer composites are complex. In fact, the reinforcing mechanisms of the particulate-filled polymer composites is usually not singular, while the reinforcing mechanisms are possible twice even triple. In other words, the reinforcing effects may be provided by multiple factors, this is the synergistic

reinforcing effect theory. For instance, as to spherical particle filled polymer composite, owing to the interfacial adhesion between the filler and matrix is relatively weak, the major reinforcing mechanisms should be the results of joint actions by the filler inducing crystallization reinforcing effect and the filler frame reinforcing effect, while the interfacial adhesion reinforcing mechanism might be less important. It is, therefore, usually difficult to explain perfectly the reinforcing effect of inorganic particles to polymer materials only using singular reinforcing theory in fact. In other words, the above reinforcing theories can be combined according to specific situation including composite type, so as to interpret more accurately the reinforcing mechanisms of the composite system. [21]

Even though there are different reinforcing theories used to explained the effect of nanoparticle addition into a polymer matrix it is concluded that in order to define fully this effect it is important to consider all the above mentioned reinforcing theories. Any model used to analyze this reinforcing effect must be able to consider all the theories in order to be used for practical application.

1.3.4 Toughening mechanism and Fracture in Polymer nanocomposites

Strength and toughness are very much interlinked, with toughness usually being more important than strength. Soft or hard particles of a wide range of shape and size can toughen glassy polymers. In polymer nanocomposites while soft and hard near spherical particles can, in the right size volume combination, increase the toughness, high aspect volume ratio in general do not significantly toughen the polymer and in many cases cause significant embrittlement. [18]

In their desire to characterize toughness of ductile polymer nano-composites more exactly, many researchers have turned to fracture mechanics. It is generally appreciated that fracture initiation at high stress cannot be explained by linear elastic fracture mechanics. However, the post yield fracture mechanics J-integral approach, used by many to characterize the toughness of ductile polymer nanocomposites, has many limitations. More importantly ductile semi crystalline polymers and their nanocomposites often exhibit considerable crack growth resistance before the fracture becomes unstable. Crack growth resistance is known to be size and geometry dependent for other than very small crack extensions. If there is significant crack growth resistance, J is not a good measure of the toughness of a nanocomposite. [18]

The more brittle polymer nanocomposites can be characterized by the plane strain fracture toughness, K_{Ic}, obtained from well-established linear elastic fracture mechanics, though even here due attention is not always made to obtain valid K_{Ic} values, especially in regards to the specimen size, which is often minimized because the nanocomposites are usually only produced in quite small volumes. However, provided the standard test methods are strictly followed there is no real difficulty in obtaining valid plane strain fracture toughness values. [18]

An alternative was presented [23] to characterize the interfaces in epoxy-clay nanocomposites via the manner of fracture mechanics. The fracture surface may propagate in three ways: (i) Mode I crack opening mode, (ii) Mode II crack e sliding mode and (iii)Mode III crack e tearing mode. In this study, full atomistic models of these interfaces are constructed and they are subjected to Mode I separation to obtain the traction stress versus separation distances relations. Mode II and III separation not considered. The traction separation relations obtained in this manner makes no prior assumption of the crack evolution. Even for interfaces with multiple phases, the fracture surface would correspond to the least energetic one. Key parameters such as peak strength (for damage initiation criterion), fracture energy and final failure separation distance (for post damage evolution) can be quantified from the traction separation curves which can then be used to parameterize the interfaces in continuum models. [24]

There are a few analytical models based on the crack propagation along the particle surfaces taking the interspacing between the particles into account as well as mathematically considered trapping, pinning and bridging of the crack front on the particles It has been shown that the fracture phenomena of the composites filled with nanometer-sized particles differ from the behavior of the composites filled with micrometer-sized or larger filler particles. [24]

Multiscale simulation, from the nanoscale to the macroscale or in the reverse order, has the capability to help better understand the toughness mechanism. To investigate the influence of nanotubes in crack propagation, two problems are considered. In the first problem, the effect of weight percentage and nanotube direction with respect to crack and in the second, the influence of several parameters such as type, length, diameter, chirality on fracture are studied. [24]

Even though it has been reported that the fracture toughness of a polymer matrix can increase with the addition of nano-particle, the addition of a hard particle component to a ductile polymer matrix

may lead to an embrittlement of the resulting composite, if the volume percentage of the reinforcing particle is not low enough. It has been reported that up to 5 volume % addition of a nano-particle could increase the fracture toughness of polymer matrix up to 700%. Again this will also depend on the size of the nano-particle and it is also reported the smaller the particle the better. This fact been well recognized the behavior of fracture in nano reinforced polymer matrix and how to model and analyze it is steel an area of research that needs a lot of work.

1.3.5 Modeling

In the recent years, many attempts have been made to realize and characterize the parameters which govern the structure–property relationship in the polymer nanocomposites. It is well known that many factors related to nanofiller including volume fraction, aspect ratio, strength and dispersion quality as well as the properties of interfacial/interphase region between polymer matrix and dispersed particles such as the size (diameter) and strength significantly change the mechanical properties of CPN. [25]

Molecular simulations are now routinely employed to study phenomena on the molecular level and quantitatively predict physical properties of nanometer sized constituents. They are increasingly accepted as an effective tool for studying nanostructures. Due to intensive computational requirement, the models in molecular simulations are usually limited to nanometer scale and cannot be used to simulate nanocomposites at the macroscale. Thus, molecular simulations are selectively employed to focus only on certain critical regions of the nanocomposites, such as single silicate sheets or interfaces. [26]

Tanaka et.al.(2013) calculated the binding energies between surfactants, silicate sheets and Nylon chains and they tried to build a connection between the binding energies and interfacial strength using the Griffith criterion based on the assumption that the binding energy between the silicate sheet and other molecules equals to the fracture energy needed to split the clay polymer interface. [27]

Toth et.al.(2011) calculated the binding energies between the clay particle and surrounding polymers and proposed that high interfacial binding energy is responsible for high mechanical performance of nano-composites. These previous works aim to establish a correlation between the

binding energy profiles and the overall mechanical performance of nanocomposites. However, there are no direct evidences or theories to support the hypothesis. [23]

In computational material design, the multiscale methods are powerful tools to extract the material parameters based on the fine scale details. While numerous multiscale methods were developed for intact materials, far less methods are applicable for fracture and damage simulations. Multiscale methods can be categorized into hierarchical, semi concurrent and concurrent methods. In hierarchical multiscale methods, the information is passed from the fine scale to the coarse scale but not vice versa. Computational homogenization is then a classical up scaling technique. Hierarchical multiscale approaches are very efficient to extract material properties. [28]

Recently, Pahlavanpour et.al (2011) evaluated the performance of commonly used analytical micromechanical models to predict the elastic properties of polymer/clay nanocomposites with the help of numerical simulations based FEM. The results show that the comparison between analytical and simulations revealed that the MT model is the most reliable method to be used for the possible ranges of modulus contrast, aspect ratio and volume fraction. [15]

Lielens et.al (2012) give a best prediction compared to MT model at high volume fractions when the rigidity contrast between effective particle and polymer is also high. The SC scheme overestimates the axial Young's modulus for all studied cases of PCN (polymer clay nanocomposites). [29]

Odegard et.al (2013) proposed the effective interface model (EIM) in order to generalize the micromechanical models of composites onto nanocomposites. Here, they develop a computational finite element micromechanical model based on the effective interface model. In this model, the homogeneous region of finite size represents molecular structure of the perturbed polyimide and interfacial molecules with a gradual transition to the bulk molecular structure. The ‘‘effective interface layer’’ is considered here as a region of finite thickness around nanoparticle, which contains inter phases, and/or other structural deviations, or has atomistic structures and properties different from those of both matrix and particles. [30]

The complete exploitation of the benefits deriving from nano modification requires convenient models to soundly predict the macroscale mechanical properties starting from the material nanostructure in order to nano design the best material solution for a specific application.

Unfortunately, modeling the effects of damage at the Nano scale on macro scale properties is far from easy. This is mainly because at that length scale classical micromechanics is no longer valid and a complex multi-scale strategy is necessary in order to properly describe the nanocomposites material behavior, physically and mathematically, in each individual scale of interest. Moreover, a basic step toward this challenging goal is the knowledge of the dominant nano scale damaging mechanisms which might sensibly differ depending on the type, the morphology and the fictionalization of the nanofiller.

1.3.5.1 Multiscale modeling

There are two types of approaches or steps of multiscale modeling, the bottom-up and top-down. In the bottom-up analysis method, one firstly obtains the effective material constants using a low-scale such as Nano, meso or micro RVE model, then applies it in the high-scale FE simulation in which the material is assumed to be equivalently homogeneous according to the theory of continuum mechanics. This approach has been applied extensively in conventional composite analysis. In the top-down or global–local method, one firstly finds the properties in the local region of a macro-scale sample under practical loads, then applies the resultant loads or displacements on the boundary of a smaller region as a new input (i.e., the global–local modeling technology which has been explored in macro-scale applications of structural analysis. The advantage here is that the model can accurately reflect the load and boundary conditions according to the experimental setup. [24]

1.3.5.2 Multi-steps homogenization procedures

The modeling is carried out on three levels. At Nano level the composite consists of three phases: matrix, nanoparticles and interphase zone around the particles, considered as additional phase. The properties of this transition zone are not constant and vary from the properties of the inclusion at the inner boundary to the properties of the matrix at the outer boundary. The transition from nano to micro level is realized over a homogenization procedure. It transforms the nano inclusion and its surrounding interphase area into a single homogeneous particle with new properties, accounted further on micro level. At micro level the material considered is a multiphase particle reinforced composite with size sensitive matrix. At this level a two-step homogenization procedure is realized. At macro level we deal with an isotropic Cauchy type mono-phase material is obtained after homogenization. [12]

The model suggests that not only the existence of inter phase zone with a particular width, but the size of inclusions itself influences the properties in the intermediate zone. The smaller the inclusions, the stronger the interphase layer. [12]

As mentioned by different articles, by different refreshers this approach, the multi-step homogenization procedure, is found to be very reliable technique to predict the homogenized material properties of nano-reinforced composites.

1.3.6 Manufacturing of Polymer Nano-composites

Many methods have been described for the preparation of polymer nanocomposites, including layered materials and those containing CNTs. The most important ones are i) Intercalation of the polymer or pre-polymer from solution; ii) In-situ intercalative polymerization; iii) Melt intercalation; iv) Direct mixture of polymer and particulates; v) Template synthesis; vi) In-situ polymerization; and vii) Sol-gel process. [17]

Intercalation or Prepolymer from solution is employed for layered reinforcing material in which the polymer may intercalate. Use of solvent in which the polymer or the pre-polymer is solvent and the silicate layers are swellable. [31]

In-situ Intercalation Polymerization, is a process done by encasing of the layered silicate within the liquid monomer or a monomer solution resulting in the formation of polymer between the intercalated sheets. Polymerization by heat or radiation, by diffusion of a suitable initiator or by a catalyst fixed through cation exchange inside the interlayer, before the swelling step. [31, 32]

Melt Intercalation is done by annealing of a mixture of the polymer and the layered host above the softening point of the polymer, statically or under shear. Diffusion of polymer chains from the bulk polymer melt into the galleries between the host layers during annealing. [33]

Template Synthesis, is in situ formation of the layered structure of the inorganic material in an aqueous solution containing the polymer. The water soluble polymer acts as a template for the formation of layers. Widely used for the synthesis of LDH nanocomposites, but less developed for layered silicates. [32]

Mixing or Direct mixture of polymer and particulates mixing of either polymer or monomer with reinforcing materials and polymerization of the mixture by addition of an appropriate catalyst.

Processing of this material can be done by conventional molding technologies. Use of ultrasonic for dispersion in the polymer matrix. [14, 32]

Sol-Gel Process involves embedding of organic molecules and monomers on sol-gel matrices; introduction of organic groups by formation of chemical bonds. In-situ formation of sol-gel matrix within the polymer and/or simultaneous generation of inorganic /organic networks. [33]

Despite the successful use of these different methods for the preparation of polymer-based nanocomposites, information on various factors is still lacking, such as i) the use of an appropriate method for a specific matrix-reinforcement combination or ii) the maximum amount of reinforcements to give optimum property combinations and lower the cost of the processes, etc. Therefore, it is still necessary to look into these aspects including use of simulation and modelling techniques.

1.3.7 Polymer Nano composite gear

Gears are used to transmit motion and/or power. In recent years, polymers are replacing metallic materials in light-duty applications such as measuring instruments, medical instruments, computer peripherals, office printing machines, and automatic teller machines, due to light weight, corrosion resistance, easy manufacturability, and able to run under dry condition. Many experimental and theoretical studies were conducted on the performance of metallic gears. However, there are only a few literatures available on the performance of polymeric gears. [5]

Polymer gears have unique advantages over metal gears: low-cost and weight; high efficiency; quietness of operation; functioning without external lubrication; etc. There would be major impacts on automotive and aerospace engineering as well as others if the gear could be used for higher power transmissions. However, the main limitations of their application are to understand: their performance under relative high load conditions; their complex thermal mechanical behavior; their hyper elastic and visco elastic behavior. [34]

Polymer and polymer nanocomposites gears are now considered for applications from low-power, precision motion to high power transmission, even in such challenging environments as healthcare and automotive engineering. For example, there are reports in automotive engineering of a 70%

reduction in mass, 80% reduction in inertia and up to 9% reduction in fuel consumption by using polymer gears instead of metal. [10]

When the loading is significant, for example in the automotive industry, rating techniques derived from metal gear practice are usually used to arrive at a design. Currently, there are a number of national and commercial standards and design methods for polymer composite gears, e.g. British Standard and Polyphenol. However, it may be noted that the quoted allowable endurance limits for bending and contact stresses are mainly given for acetal and nylon. With so many new plastic materials and filler combinations becoming available, this limited data is a major shortcoming. Furthermore, none of those standards correlated well with the test results and the polymer composite gears' potential use in power transmission is limited due to the lack of understanding of their behavior under load as well as physical limits created by the low strength of polymer. A great number of experimental works involved meshing polymer gears with steel pinions, e.g. nylon against steel. Since accurate molded gears are now available, it is necessary to learn more about the performance of these gears under different operating conditions. [35]

A wide variety of different types of polymer materials (PA, POM, etc.), different reinforcements (carbon fiber, glass fiber, nanoparticles, etc.) and internal lubricants (PTFE, MoS2, etc.) can be used to tailor a polymer for a specific application. However, due to the large number of different materials available, it is very difficult to determine the optimal material combination for a specific gear drive, especially when also considering noise and vibration properties. [36]

Even though polymers and their composites offer a great advantage as compared to conventional gear materials their application has been limited due to a luck of data and research available. To fully use polymer composites gear for medium and high power application different analytical and experimental works are required.

1.3.8 Main failure modes for polymer nanocomposite gear

Potential use of polymer composite gears in power transmission is limited by a lack of fundamental understanding of their actual mechanical and, especially, thermal behavior. To evaluate how much power a polymer composite gear can transmit, it is essential to investigate the thermal fatigue strength and wear resistance of the gear. [37] There are four highly typical failure modes in polymer gears, wear, pitting, root and pitch cracks: The failure mechanism depends on the testing

conditions (load, speed and temperature) and material combination. [36] While similar failures can occur in metal gears, the underlying failure mechanisms in polymer gears are dominated by thermal factors; this is not the case with metal gears. [10]

Surface cracks were dominant in unreinforced gears subjected to low stresses. Severe deformation was observed at higher stress levels. Reinforced gears exhibited longer life compared with unreinforced gears due to their superior mechanical strength and thermal resistance. An increase in tooth temperature decreases polymer mechanical properties and also decreases the performance of the gear pair. The enhancement in mechanical properties of polyamide nanocomposite gears results in higher power transmission efficiency compared to unreinforced polyamide gears. [38, 10]

It has been known that one of the dominated failure forms for polymer composite gears is thermal wear failure caused by gear surface contact friction and polymer low heat conductivity. The polymer gear contact surface temperature is so high resulting in local softening and surface wear is increased dramatically. [39]

However, a detailed understanding of this sensitivity and of how their mechanical properties degrade with increasing temperature is lacking in the literature. Understanding their thermo-mechanical behavior remains very challenging because of the severe non-linearity and high real-life sensitivity to small changes in polymer gear temperature.

1.3.8.1 Gear Body temperature

Since it has been identified that low temperature resistance is the main reason for failure researchers have attempted to reduce the gear tooth surface temperature by increasing the tooth width in single tooth contact region. Providing a hole on the gear tooth reduces the surface temperature and it is further reduced by steel pin inserts. Providing a hole in gear tooth reduces the tooth stiffness and leads to large tooth deflection. Heat dissipation through the hole is effectively achieved only through the proper selection of size of the hole and location. Significant reduction in surface temperature and wear is achieved by drilling multiple radial and axial cooling holes. The performance of a gear pair depends upon the material, geometry, speed, loading condition and friction. The repeated bending of gear tooth leads to hysteresis heat generation. The power loss

due to hysteresis mainly depends on the material dissipation factor, also called as loss tangent, and load. [5]

The difference in gear efficiency of polymer nanocomposite gears with different weight percentage of nano-particles is more significant at higher torque level compared to lower torque levels. The addition of nano-particles reduces the ductility of the polymer but increases the gear efficiency. Further research could be made to find most appropriate weight percentage of Nano-particle in polymer matrix and different Nano-size particles to get further enhancements in gear efficiency. The dynamic mechanical analysis (DMA) of the PA6 and PNC materials reveals that the PNC has higher storage modulus and higher temperature resistance compared to PA6. [5]

Mathematical models were developed and reported to quantify the amount of heat generated due to friction and hysteresis loss in polymer gears during meshing. The rotational speed of the spur gear affects the performance of unreinforced and glass fiber reinforced spur gears. Initial application of grease significantly reduces the tooth wear in carbon fiber reinforced poly-ether-ether-ketone gear and carbon fiber reinforced polyamide gear. A new design method based on the relation between the wear rate and its surface temperature was developed for acetal gear. [5]

The existing gear surface temperature predictions require further study to be used for practical applications. For instance, Hachman and Strickle's equation was based on the assumption that a lubricant does not contribute significantly to the heat transfer from the tooth. This is not the case when gears continuously lubricated with oil. Except for Garvin et al.'s equation, temperature equations are complicated and inconvenient to use in practice and also Garvin's equation is limited to polymer against steel gears. Most of the existing methods for surface temperature measurements are carried out after stopping the gears and they are inaccurate since the flank temperature drops very rapidly once the gear stops. [40]

Takanashi developed gear temperature equations that contain not only friction generated heat, but also heat generated from gear deformation. The proved to be precise enough for practical application. However, several of the parameters needed for the calculation of the deformation part are difficult to determine. The model was developed using a pair of plastic and metal gears; therefore, it has limited value for pairs of plastic gears. Determination of the gear temperature during meshing is an indispensable step for the precise calculation of plastic gears. The existing

models for temperature calculation can give a rough estimate, but they do not provide reliable results. Particularly for the meshing of new material pairs, there is a lack of specific material data.

K.Mao et.al presented accelerated test model temperature calculations using the Hachmann–Strickle temperature model, however with corrected and improved input parameters, which were determined from the test results and was found to be correlate well with the test results. [36]

As it is mentioned the main failure mode for polymer gears is their low resistance to temperature, which is related to the property of polymers. This property can be enhanced by the addition of nano-particles and may researches support this. But the prediction of surface temperature of the gear tooth is an area that needs more work and validation using both experimental and analytical data.

1.3.8.2 Wear

Wear forms occur because of the direction of the relative movement that occurs as the teeth enter and leave the mesh. Sliding is away from the pitch line on the driving gear and toward the pitch line on the driven gear, giving rise to the particular wear pattern. A typical worn tooth profile consists of two scalloped wear zones, one starting from the tip and running to the pitch point and the other going from the pitch point to the root. [37]

In addition to direct material loss, which leads to functional failure, wear of the surface causes the gear system to significantly modify its characteristics of vibration and noise. The mesh excitation is highly sensitive to the surface geometry. The wear surface affects the gear contact patterns such that the contact stresses and load distributions are changed to accelerate the appearance of other failure modes.

A large number of parameters must be considered to accurately describe the characteristics of the wear of surfaces in contact with each other. Mechanisms of wear are even more complex than the contact parameters, such as the radii of curvature, slip rates, and normal load range with the contact location. In addition, other contact parameters that affect the conditions of elasto-hydrodynamic lubrication (lubricant parameters and surface roughness characteristics) are among the parameters of interest for gear wear.

According to Flodin and Andersson, rolling gear teeth interact and slide against each other under high contact pressure. High-performance gears are generally lubricated with oil or grease. The state of lubrication is most likely in the boundary or mixed system, meaning that the lubricant film generated is not always sufficiently thick to separate the interacting surfaces.

Sliding wear at point P on a dry contact or a mixed lubricated boundary surface can generally be regarded as a function of the initial value and described by a differential equation. The accumulated wear at a point P can be determined by Archard's wear equation: Although many researchers have proposed more advanced wear models using different methodologies and parameter sets, Archard's wear model remains the most commonly used model for practical applications, such as cam-follower contacts, engine piston rings, and gear contacts, where the geometry and operating conditions are already complex. [41]

Acetal gear friction and wear performance was found to be entirely dependent on surface temperature at high loads. A sudden transition to high wear rates was noted as the transmitted torque was increased to a critical value. The gear surface will wear slowly with a low specific wear rate if the gear is loaded below the critical value. The critical torque is associated with the gear surface temperature of the material reaching its melting point. A comprehensive investigation on acetal gear surface temperature has been carried out and acetal gear transition point (critical torque) has been predicted based on the gear surface temperature predictions for given geometry and running conditions. This approach of critical load for acetal gear has been applied to the experimental applications and good agreements have been achieved between the prediction and test results. [42]

As it is discussed above wear is one of the main failure modes of polymer gears, and this is mainly due to the low thermal resistance of polymers. Archard's wear equation is the preferred method of predicting the wear depth of polymer gears. It modified form, so as to make it suitable for gears has been used in many literatures and found to correlated well enough with the experimental results.

1.3.8.3 Fatigue

Gear teeth are subjected to alternate stresses at various points. This process can lead to failure by fatigue even if the elastic limit of the material is not exceeded. In particular, gears often break due to crack propagation in the tooth root.

Design engineers use the Palmgren–Miner law, the linear damage rule (LDR), and its modifications to predict the fatigue life of components in the case of variable loading. [41]

The best source of information about the fatigue life of one part comes from either the normalized testing of specimens or the real part testing. Both methods have the same shortcoming; they are lengthy and require a significant amount of scarified parts. When using data from normalized specimens, the values must be adjusted to consider the differences between the specimen and part. Some examples of differences to be considered in the specific case of gears are the particular shape, load application, size and operating temperatures. Coefficients that consider these factors are often called “fatigue reduction coefficients” and multiply the theoretical fatigue value to obtain the real value. [18]

Additionally, these coefficients are often designed to be used with metal parts, and results using this methodology can be misleading without proper validation given the various particularities that distinguish plastic gear meshing from metal gear meshing. [43]

Surfaces subjected to rolling and sliding contacts may suffer from contact fatigue; the mechanism causing rolling contact fatigue to initiate and propagate is not fully understood. There are a number of differences between classical fatigue and RCF that make it impossible to apply the results from classical fatigue to RCF directly. [41]

Few studies have compiled results of the experimental factors of the surface fatigue material properties for plastic gears. Unfortunately, there is not sufficient data in the literature regarding the contact fatigue properties of plastic gear materials. [41]

As it is mentioned the most reliable data for fatigue life of a material is obtained from experimental work, but analytical approaches are also used depending on the situation. To obtain accountable results, we use validated experimental data from the literature of gears having the size and material

properties in the range of our model scope. This approach avoids errors induced by one or more inappropriate coefficient.

1.4 Statement of the problem

Polymers have inferior mechanical and thermal properties as compared to conventional gear materials. Previous works show that polymer mechanical and thermal properties like wear resistance can be improved by Nano particle reinforcement. Even though some work has been done by different researchers there is steal a need for more analytical and experimental work to be done in this area especially the application of this composites for different mechanical components like transmission gears.

For this research among the different types of polymers used for gear manufacturing acetal reinforced with Nano silica is selected for modeling and perform numerical analysis, for wear and thermal as well as fatigue life analysis.

Improvement in the above mentioned properties is expected at the end of this research.

1.5 Objective of this research

1.5.1 General objective

The general objective of this research is to show the advantage of Nano particle reinforced polymer gear for improved mechanical and thermal properties by using homogenization procedure to predict the mechanical property and simulation software Abaqus/CAE 6.14 to check the performance.

1.5.2 Specific objective

The specific objective of this research can be summarized as follows;

- The homogenized material property that results due to nano particle (spherical) addition in to the polymer matrix will be identified using multi-steps homogenization approach.
- The mathematical modeling of the homogenization procedure will be performed using MATLAB.
- The most appropriate analytical approach to predict the wear, thermal and fatigue life of the composite gear will be identified.
- The temperature, wear and fatigue resistance of the gear designed and simulated using acetal nano-silica composite will be checked.

- The results found will be compared with previously found experimental data for pure acetal gear.

1.6 Organization of the paper

This thesis work is organized in to five chapters. The first chapter, includes introduction which gives some background information on the overall idea behind this work, statement of the problem based on the existing gap that is observed, general and specific objectives to be achieved at the end of this work.

The second chapter includes, a review of literatures relevant to this thesis work, which can lay the background for the work to be done are mentioned

In chapter three the methodology applied, the assumptions considered, the materials selected, analytical methods in modeling of the composite material, and the analytical methods in wear, surface temperature change and fatigue life analysis for plastic gears is discussed. Also the steps followed in order to simulate the gear model on Abaqus/CAE software are discussed in detail.

In chapter four the results of the analysis, for the homogenized material property as the well the wear, thermal and fatigue life analysis are given using the simulation results obtained from Abaqus simulation. It also includes different plots to illustrate the results and the meaning of the results is discussed comparing it to a previous work and result.

In chapter five, conclusions based on the result are made. Recommendations are also given, as well as future works to be done on this area are suggested.

Chapter Two

2. Analytical Methods and Conditions

2.1 Material

The material used for this research is polymer, acetal, reinforced with nano-silica, and the material properties of this components which are required to get the homogenized material properties by the approach which is going to be discussed letter are as shown in the table below.

Material	Elastic Modulus(MPa)	Shear Modulus(MPa)	Poisson's ratio	Density(g/cm^3)	Thermal conductivity(W/cm.K)
Acetal	1400	520	0.35	1.41	0.0036
Silica	70,100	25,000	0.3	2.2	0.014

Table 2. 1. Material properties Acetal and Nano-Silica

2.2 Modeling the composite material

As briefly mentioned in the literature review the composite material is modeled using multi- scale homogenization approach in order to determine the new properties of the composite. The modeling is done in three levels starting at the nano level and proceeding to the micro level.

2.2.1 Modeling at the nano level

The matrix is considered as micropolar elastic material which is the same at Nano and microscales and will be described in the next section. Let the composite contain *m different spherical Nano phases* with corresponding diameters $d_j = 2r_j, j = 1 \dots, m$. As the inclusions are much harder compared to the matrix, they are assumed pure elastic. The *shear (* G_j^{nan} *) and the bulk modulus (* K_j^{nan}) of the non-inclusion are:

$$G_j^{nan} = E_j^{nan}/2(1+\nu_j^{nan}), \qquad K_j^{nan} = E_j^{nan}/3(1-2\nu_j^{nan}) \quad \text{.....Equation 2.1}$$

The *transition zone* around each particle is assumed of Nano size a which can be generally function of the matrix and of the inclusions properties. In case of polymer matrices this intermediate zone depends on manufacturing conditions. According to investigations published in literatures , a is approximately constant and independent on the nanoparticle size d_j. The properties of this transition zone are influenced strongly on the particle properties, therefore the material

inside it is assumed elastic too. The width of the interphase layer is restricted by the half of the surface-to-surface interparticle distance, i.e. the model does not consider overlapping of interphase zones. *The parameter β_g enables the physical–chemical interaction between fillers and matrix to be taken into account.* Its value can be obtained from the equation below

$$\beta_g = 1 + \frac{d_{mean}^2}{2a\langle L\rangle} \quad \text{Equation 2.2}$$

Where d_{mean} is the averag diameter of particles and $\langle L\rangle$ is the averaged surface to surface interparticle distance. The interparticle distance $\langle L\rangle$ depends on volume fraction, shape, arrangement and size distribution of the particles.

$$\langle L\rangle = d_{mean}\left[\left(\frac{C_{summax}}{C_{filler}}\right)^{1/3} - 1\right] \quad \text{Equation 2.3}$$

C_{summax} and C_{filler} will be discussed later.

If the interphase region is divided into q concentric subareas, *the properties in the interphase region* are defined with:

$$\left.\begin{aligned} E_k^{(j)} &= E_o + (E_j^{nan} - E_o)\left(\frac{r_j + a + r_k^{j)}}{a}\right)^{\beta_g} \\ r_k^{(j)} &= r_j + a\left(1 - \frac{k-1}{q}\right) \\ \nu_k^j &= \nu_o \end{aligned}\right\} \quad \text{Equation 2.4}$$

Each nanoparticle with its interphase zone is subjected to homogenization and the properties of the obtained equivalent inclusion are determined. In our case a self-consistent homogenization procedure is applied to the (q + 1)-phase material. According to it the properties K_j and G_j of each equivalent inclusion with diameter $D_j = 2(r_j + a), (j = 1, \dots, m)$, originated from nanoparticle j and its surrounding, are solution of the nonlinear equations system:

$$\sum_k^{q+1} \frac{C_k^{(j)}}{1-\frac{3K_j}{3K_j+4G_j}\left(1-\frac{K_k^{(j)}}{K_j}\right)} - 1 = 0$$

$$\sum_k^{q+1} \frac{C_k^{(j)}}{1-\frac{2(3K_j+6G_j)}{5(3K_j+4G_j)}\left(1-\frac{G_k^{(j)}}{G_j}\right)} - 1 = 0. \quad \text{.....Equation 2.5}$$

In the above expressions $K_k^{(j)}\left(E_k^{(j)}, \nu_k^{(j)}\right), G_k^{(j)}\left(E_k^{(j)}, \nu_k^{(j)}\right), (K = 1 \ldots . q)$ are obtained from expressions analogous to (Eqn. 2.1) and $K_{q+1}^{(j)} = K_j^{nan}, G_{q+1}^{(j)} = G_j^{nan}$ and the volume fractions of the phases are:

$$C_k^{(j)} = \frac{\left(r_j + a\frac{q-k+1}{q}\right)^3 - \left(r_j + a\frac{q-k}{q}\right)^3}{(r_j+a)^3}, \quad k = 1, \ldots . , q \quad \text{..... Equation 2.6}$$

$$C_{q+1}^{(j)} = \left(\frac{r_j}{r_j+a}\right)^3$$

As a result of the described procedure we obtain m homogenized phases of equivalent inclusions with diameter $D_j = d_j + 2a$.At the higher structural level, the micro level, they will be considered in the same way as other reinforcing phases on this level.

2.2.2 Modeling at micro level

2.2.2.1 Modeling of the hardening phases

The hardening particles at this level are assumed elastic spheres with different diameters and mechanical properties. They can be grouped in a finite number $n > 2$ of sets, according to the diameters $D_i (i = 1, \ldots, m, m+1, \ldots . , n)$. The first m sets are the result of the homogenization procedure at Nano level. The volume fraction of each set is C_i. The total volume fraction of the hardening phases (equivalent inclusions) is:

$$C_{sum} = \sum_{i=1}^{n} C_i = C_{nano} + C_{intphs} + C_{micro} \quad \text{..... Equation 2.7}$$

We consider the material of the inclusions as Cauchy-type elastic isotropic one with mechanical characteristics: E_i, ν_i, G_i and K_i. The number of hardening phases should not exceed n.Everywhere in the paper the subscript 0 stays for the matrix and the subscript i– for the phase i.

It should be mentioned that no matter what is the size $D_i = (i = 1, \dots, m)$ of the equivalent inclusions, their interaction with the matrix is already taken into account by the modeling at the lower structural level and there is no such influence at that level.

2.2.2.2 Modeling of the matrix material

The matrix of the multiphase composite is considered as micro polar elastic–plastic Cosserat continuum. The stress and strain measures are the stress tensor $\sigma_{ij} = \sigma_{(ij)} + \sigma_{\langle ij \rangle}$, the couple stress tensor $m_{ij} = m_{ij} + m_{\langle ij \rangle}$, the strain tensor $\varepsilon_{ij} = \varepsilon_{(ij)} + \varepsilon_{\langle ij \rangle}$ and the curvature tensor $k_{ij} = k_{(ij)} + k_{\langle ij \rangle}$. Symbols (. . .) and ⟨……⟩, in the subscript denote the symmetric and anti-symmetric parts of a tensor respectively. The study is restricted to isotropic Centro-symmetric micro polar continuum. The elastic behavior of the matrix material is described with the well-known relations

$$\sigma'_{(ij)} = 2\mu_o \varepsilon_{(ij)} \qquad \sigma_{\langle ij \rangle} = 2\kappa \varepsilon_{\langle ij \rangle} \qquad \sigma_{(kk)} = 3K_o \varepsilon_{(kk)}$$

$$m'_{(ij)} = 2\beta k'_{(ij)} \qquad m_{\langle ij \rangle} = 2\gamma k_{\langle ij \rangle} \qquad m_{(kk)} = 3N k_{(kk)} \qquad \text{……..Equation 2.8 1}$$

$$K_o = \lambda_o + \frac{2}{3}\mu_o \qquad N = \alpha + \frac{2}{3}\beta$$

Where

$$\lambda_o = E_o \nu_o / [(1 + \nu_o)(1 - 2\nu_o)] \quad \text{…… Equation 2. 9}$$

and μ_o are the elastic Lamé constants, α, β, γ and κ are the Cosserat material constants. K_o and N are Cauchy and Cosserat bulk moduli respectively, E_o is Young's modulus and ν_o is Poisson's ratio. Everywhere in the paper (. . .)' means deviator. $G_o = \nu_o$ is Cauchy shear modulus.

The elastic characteristic length parameters for Cosserat media can be defined in different ways. New assumptions for the relation between the intrinsic length and the Cosserat moduli of the matrix material are used here:

$$l_1^2 = \frac{\alpha}{\lambda_o} \qquad l_2^2 = \frac{\beta}{\mu_o} \qquad l_3^2 = \frac{\gamma}{\kappa} \quad \text{…… Equation 2. 10}$$

In order to ensure smooth transition from elastic to plastic state the following condition is adopted:

$$l_1 = l_2 = l_3 = l_m \quad \text{…… Equation 2. 11}$$

2.2.3 Transition from micro to macro level in the case of low filler volume fraction

Consider the case when all hardening (no matrix) phases have equal properties K_{inc} and G_{inc} and are of the same shape, described by the size parameter D. If experiments show that too many sizes of inclusions exist, their grouping in a finite number of sets is not advisable. In such a case it is preferable to define $\Psi(D)$ and $\psi(D)$, such that $d\Psi(D) = \psi(D)dD$ and $\int \psi(D)dD = 1$. Note that if the interphase width is equal for all nanoparticles the size distribution function of nanoparticles $\psi(d)$ is of the same type as w(d) and is shifted with $2a$.

The infinitesimal volume of a pseudo grain, containing inclusions with size parameter D can be defined as $d\Omega(D)$. This pseudograin contains a volume d VD of inclusion of size D. On the other hand, the total volume of inclusions in REV is $V_{inc} = \int dV_D$. The distribution functions are defined with:

$$\frac{dV_D}{V_{inc}} = d\Psi(D) = \psi(D)dD. \quad \text{Equation 2. 12}$$

If experimental observations show that the distribution function obeys the normality conditions, it may be taken in the form:

$$\psi(D) = \left(2\pi\sigma_\psi^2\right)^{\frac{-1}{2}} exp\left[-\frac{(D-\mu_\psi)^2}{2\sigma_\psi^2}\right] \quad \text{Equation 2. 13}$$

where μ_ψ and σ_ψ^2 are the mean and the variance respectively.

A rough estimation of distribution characteristics can be obtained as follows:

$$\left.\begin{aligned}\mu_\psi &\approx \frac{1}{2}[D_{max} + D_{min}],\\ \sigma_\psi &\approx \frac{1}{6}[D_{max} - D_{min}],\end{aligned}\right\} \quad \text{Equation 2. 14}$$

For a given density distribution function defined by (13), the relations for the shear and bulk modulus of the composite can be given as:

$$\left.\begin{aligned}K_c(D) &= K_o\left[1 + \frac{(1-C_o)(K_{inc}-K_o)}{C_o a_o(K_{inc}-K_o)+K_o}\right].\\ G_c(D) &= G_o\left[1 + \frac{(1-C_o)(G_{inc}-G_o)}{C_o b_o(D)(G_{inc}-G_o)+G_o}\right]\end{aligned}\right\} \quad \text{Equation 2. 15}$$

And, the final property for the composite is the answer for the equation (16) below:

$$\int_0^\infty \frac{\psi(D)}{1-\frac{3\bar{K}}{3\bar{K}+4\bar{G}}\left(1-\frac{K_C(D)}{\bar{K}}\right)}dD-1=0,$$

$$\int_0^\infty \frac{\psi(D)}{1-\frac{2(3\bar{K}+6\bar{G})}{5(3\bar{K}+4\bar{G})}\left(1-\frac{G_C(D)}{\bar{G}}\right)}dD-1=0.$$

……Equation 2. 16

Where,

$$a_o=\frac{3K_o}{3K_o+4G_o},\qquad b_o(D)=\frac{6(K_o+2G_o)}{5(3K_o+4G_o)}$$ ……Equation 2. 17

2.3 Modeling of thermal conductivity in composites

The two basic models representing the upper bound and the lower bound for thermal conductivity of polymer nano-composites are the rule of mixture and the so-called series model, respectively. In the rule of mixture model, also referred to as the parallel model, each phase is assumed to contribute independently to the overall conductivity, proportionally to its volume fraction (ref

$$K_c=K_p\phi_p+K_m\phi_m$$ ……Equation 2. 28

On the other hand, the basic series model assumes no contact between particles and thus the contribution of particles is confined to the region of matrix embedding the particle. The conductivity of composites accordingly with the series model is predicted by

$$K_c=\frac{1}{(\phi_m+K_m)+(\phi_p+K_p)}$$ …… Equation 2. 19

Most of the experimental results were found to fall in between the two models. However, the lower bound model is usually closer to the experimental data compared to the rule of mixture.

2.4 Modeling the density of the composite

The theoretical density of polymer nano-composite materials in terms of volume fraction can easily be obtained as for the following equations given by Agarwal and Broutman

$$\rho_c=\frac{1}{\frac{w_m}{\rho_m}+\frac{w_p}{\rho_p}}$$ ……Equation 2. 20

2.5 Acetal gear specifications.

The dimensions for the gear to be simulated and analyzed for improved mechanical properties is taken from the experimental works conducted before and are shown in the table below.

Module	2mm
Tooth number	30
Pressure angle	20^0
Face width	17mm
Nominal Backlash	0.18mm
Tooth thickness	3.14mm
Contact ratio	1.65

Table 2. 2. Acetal nanocomposite gear specification

2.6 Modeling plastic gears

2.6.1 Particularities of plastic gear meshing

Plastic gear meshing presents some particularities that differ from metallic meshing. These particularities must be added to a model to properly simulate the mechanical behavior. In this section, we discuss aspects of plastic gear meshing that require attention and must be considered when a model is implemented.

Conceptually and throughout this work, it is considered that for any pair of gears studied, the movement is transmitted from one gear to the other via a pair or more of teeth touching only in a line. The contact is considered to occur at a point P (Fig 3.1) that moves along the common normal to the two base circles, also called the action line.

When the gears are considered rigid, the pair of teeth is in contact at the start point of contact “A”, where the theoretical tip circle of the driven tooth (wheel) intersects the line of action; contact ceases at end point “B”, where the theoretical contact tip circle of the drive teeth (pinion) cuts the line of action (Fig. 2.1).

For such gears, the normalized position of the theoretical contact start point following the line of action with respect to the pitch point (gear 2 as a reference) is expressed as.

$$\frac{S_2^*}{P_n} = \frac{Z_2}{2\pi \cos\theta}\left[\sqrt{\left(1+2\frac{a_2}{Z_2}\right)^2 - (\cos\theta)^2} - \cos\theta \tan\theta_f\right] \quad \text{…….. Equation 2. 21}$$

$\frac{S_2^*}{P_n}$ = normalized position of the beginning of contact.

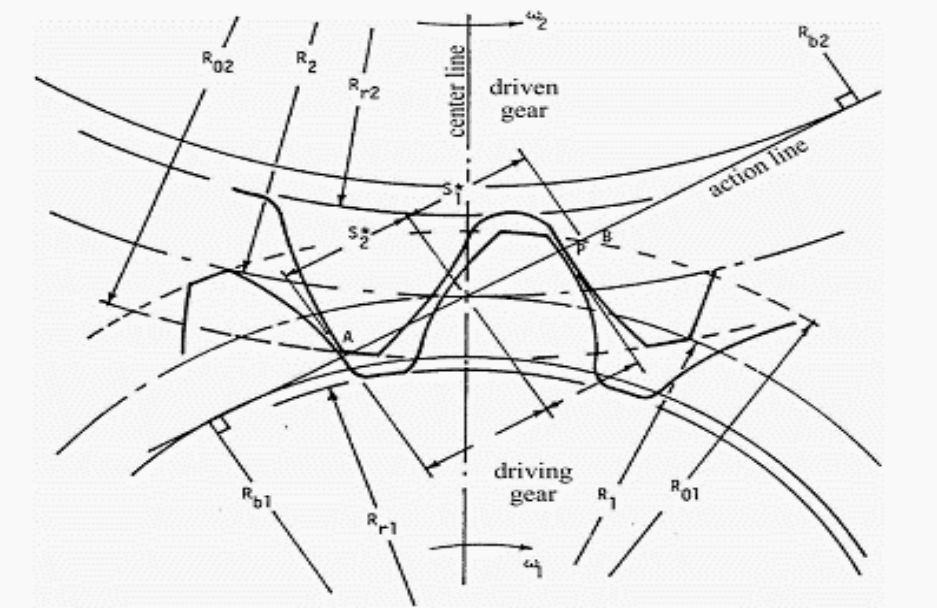

. Figure 2. 1. Theoretical spur gear load transfer points.

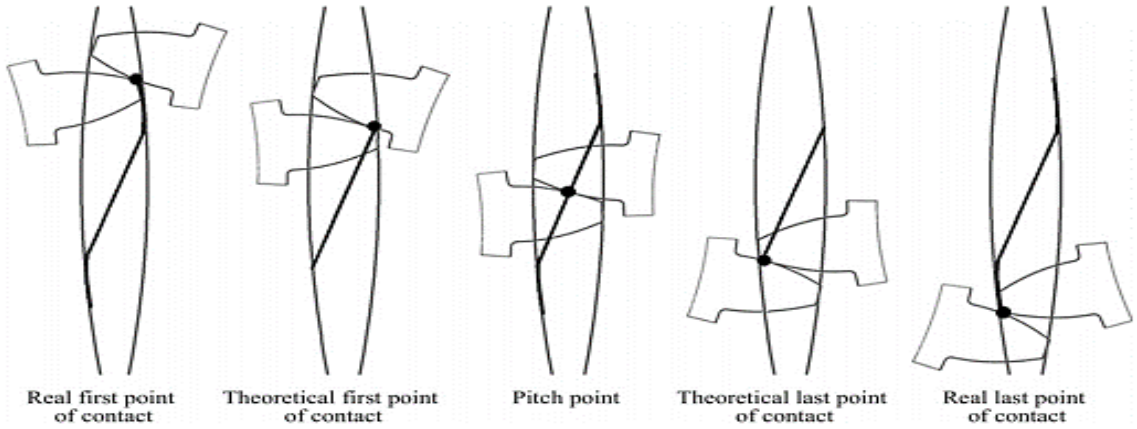

Figure 2. 2. Real and theoretical paths of contact

The expression for the normalized position of theoretical contact end is obtained from Eq. (3.21), in which the subscript 2 is replaced by 1.

By convention, when the driven gear is used as a reference,S/P_n has a negative value during the approach phase. When the contact point is below the pitch circle of the tooth of pinion 1,S/P_n has a positive value during the withdrawal phase, and the point of contact during this phase is above the pitch circle of the sprocket tooth.

2.6.2 Contact outside the line of action

When using polymer gears, the nature of the teeth causes a deformation of the pairs of teeth in contact to outside of the contact line of action. Koffi et al. established a simplified method to calculate the normalized position of the contact start point by evaluating the difference along the line of action between the theoretical contact and actual contact.

$$\frac{\delta S}{P_n} = 0.131E_2^{-0.34}\left(Z_2\sqrt{W_o P\cos\theta}\right)^{0.7}\left(\frac{Z_2}{Z_1}\right)^{-0.55} \quad \text{Equation 2.22}$$

$E_2 =$ Young's modulus at ambient temperature.

$W_o =$ specific normal load (N/cm).

$P =$ diametral pitch (m^{-1}).

Eq. (3.22) establishes a power law between the normalized deviate $\delta S/P_n$ and $W_o P\cos\theta$. Any increase in P at a constant diameter increases the number of teeth, Z, resulting in a reduction of the normal load, W_o, through the load distribution factor, W_i/W, whose value at the pitch point, W_i/W_o, decreases according to a power law with an increase in the diametric pitch, P.

The normalized increase in $\delta S_1/P_n$ and $\delta S_2/P_n$ must be combined with the theoretical contact values from Eq. (3.1):

$$\left.\begin{aligned}\frac{S_2''}{P_n} &= \frac{S_2''}{P_n} - \frac{\delta S_2}{P_n}\\ \frac{S_1''}{P_n} &= \frac{S_1''}{P_n} - \frac{\delta S_1}{P_n}\end{aligned}\right] \quad \text{Equation 2. 23}$$

The real contact ration (RCR) is then found using the equation

$$RCR = \frac{S_1^{"} - S_1^{"}}{P_n} \quad \text{.....Equation 2. 24}$$

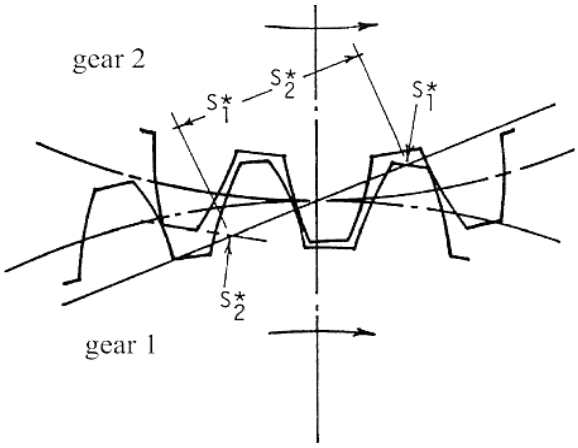

Figure 2. 3. Increase in the contact ratio with the effect of tooth deformation under loading.

2.6.3 Distribution of the transmitted normal load

The increase in the driving relation in the actual operation of two gears causes a distribution of the normal load onto more than one pair of teeth.

For practical modeling purposes, the simplified model is used; this model calculates the load distribution factor at any position during the engagement from the value of W_i/W to the original point or $W_i/W|_o$ for a plastic–plastic engagement, given by the following expression:

$$\frac{W_i}{W} = \frac{W_i}{W}\Big|_0 \cos\left(\frac{\pi}{2}\,\frac{S/P_n}{S_2^{"}/P_n}\right). \quad \text{.....Equation 2. 25}$$

2.6.4 Sliding speed

In addition to the relative rolling movement of gear teeth, the movement of a pair of contacting gear teeth comprises a sliding of one of the teeth relative to the other.

This phenomenon creates a frictional force at the contact point; the displacement of the frictional force with the point of contact causes friction losses, which result in tooth heating. The instantaneous slip velocity is defined as the difference between the instantaneous speed, on the side of the driving and driven teeth, at which the point of contact moves. Inside the line of action, the sliding speed is

$$V_s = V\left[cos\,\theta\,\frac{Z_1+Z_2}{Z_1Z_2}\,2\pi\left|\frac{S}{P_n}\right|\right].$$ ……. *Equation 2. 26*

V is the linear speed at the pitch circle

For contact outside the line of action (in the approach phase), the equation becomes

$$V_S = V\left\{\left[Z_{e1}\frac{cos\,\theta}{cos\,\theta_f}\beta\left\{cos\,\beta-\sqrt{d_r^2-(sin\,\beta)^2}\right\}-\left(1+2\frac{a_2}{Z_2}cos\,\epsilon\right)\right]^2+\left[Z_{e1}\frac{cos\,\theta}{cos\,\theta_f}sin\,\beta\left\{cos\,\beta-\sqrt{d_r^2-(sin\,\beta)^2}\right\}-\left(1+2\frac{a_2}{Z_2}\right)sin\,\epsilon\right]^2\right\}^{1/2}$$ ……. *Equation 2. 27*

With

$$Z_{e1}=\frac{Z_1+Z_2}{Z_1}$$

$$Z_{e2}=\frac{Z_1+Z_2}{Z_2}$$

$$d_r=\left[1+2\frac{a_2}{Z_2}\right]\frac{1}{Z_{e2}}\frac{\cos\theta}{\cos\theta_f}.$$

……..*Equation 2. 28*

For contact taking place outside the line of action, the sliding speed is obtained by interchanging the indices and we can reasonably assume that for the duration of the contact outside the line of action in the approach phase, tooth c2 always makes contact at its tip corner. Referring to Fig. (3.4), we write the following equation:

$$\epsilon = \psi-\left(inv\phi-inv\theta_f\right).$$ ……. *Equation 2. 29*

It can be shown that;

$$\psi\left(\frac{S_2^*+0.5\delta S}{P_n}\right)\frac{2\pi}{i_2}.$$ ……..*Equation 2. 30*

For the cosine law:

$$(r_1')^2 = r_2^2+\overline{0_10_2}^2-2\overline{0_10_2}r_2\,cos\,\epsilon.$$ ……... *Equation 2. 31*

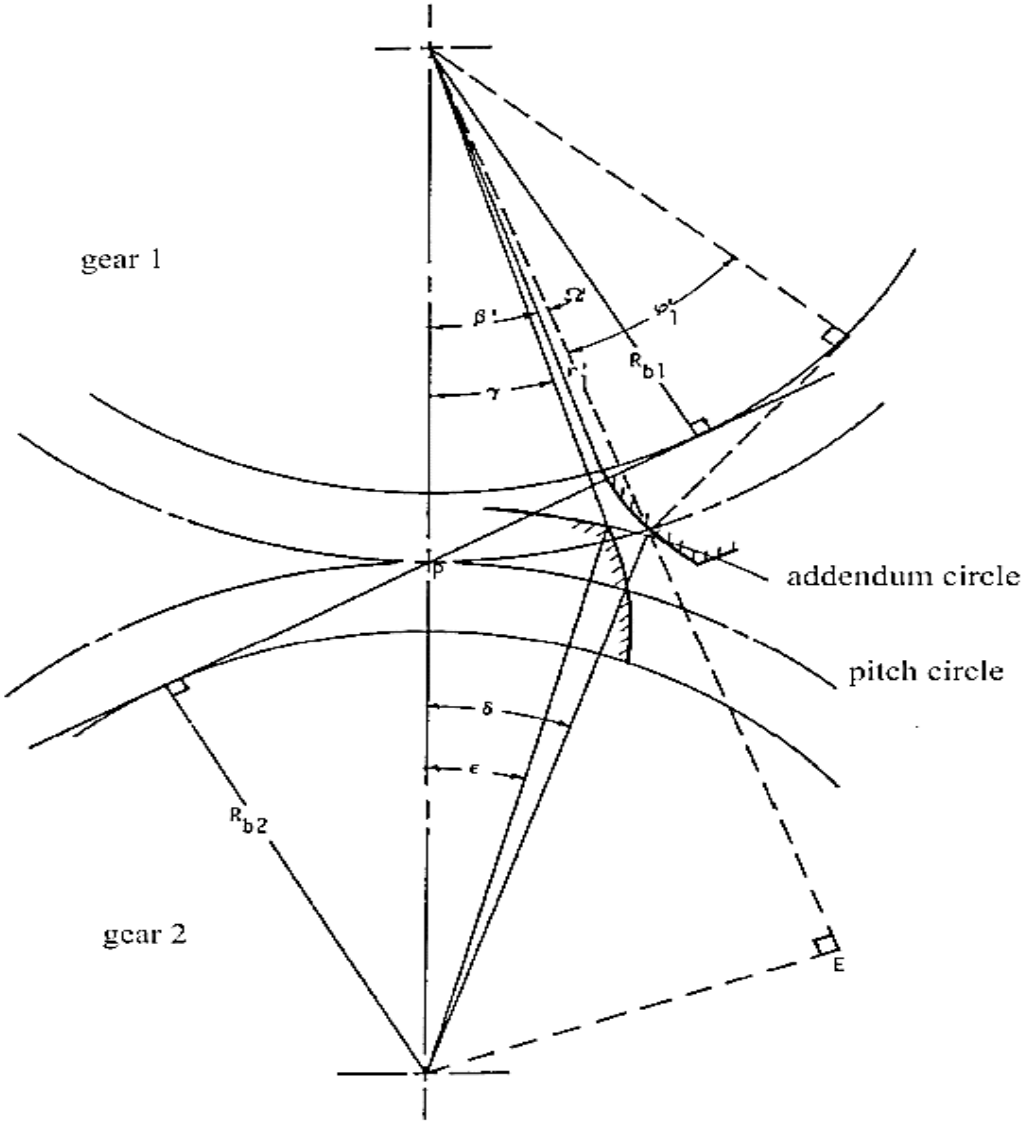

Figure 2. 4. Important angles for the calculation of [K] outside the line of action.

Once R1' has been obtained, using the sine law,

$$\beta = a\,sin\left[\frac{r_2}{r_1}sin\,\epsilon\right] \quad \text{Equation 2. 32}$$

The sliding speed V_S can be conveniently expressed using a dimensionless parameter $[K]$, as follows:

$$[K] = \frac{V_S}{V} \quad \text{Equation 2. 33}$$

The absolute value of the sliding speed increases continuously when the contact point moves outside of the theoretical bounds S_2/P_n (approach) and S_1/P_n (retreat). The first and last points of contact, $S_2^{"}/P_n$ and $S_1^{"}/P_n$, move away from the pitch point with increases in the number of teeth, Z, and the tangential load, W_t. Nevertheless, they remain stable for a (W_t/m) group (or (W_tP)), as shown by Yelle and Burns.

2.6.5 Static analysis

Constraints on gears for the transmission power can be classified into two groups: bending stresses at the root of the tooth and at the surface. These constraints are important for determining the safety factor and to evaluate fatigue.

2.6.5.1 Stress on the surface

For a given contact point, the force is not transmitted through a perfect line but rather through a small surface. This statement is fundamentally true for plastic gears due to their smaller elastic modulus.

For a given position of the contact point, the contact stress has a maximum value at the charged surface of the tooth and is near zero at the center of the tooth. This maximum value changes with the position of the contact; thus, during the rotation of a gear, each contact point undergoes the maximum contact stress only once, and the value of the contact stress depends on the expression of the maximum constraint, as follows:

$$\sigma_{0c} = \frac{1}{b}\frac{W_i}{W}W_o. \quad \text{.....Equation 2. 34}$$

From Hertzian theory, the half contact width is given by the expression

$$b = \left[\frac{4W_0}{\pi}\left[\frac{r_1 r_2}{r_1+r_2}\right]\left[\frac{1-\nu_1^2}{E_1}+\frac{1-\nu_2^2}{E_2}\right]\right]. \quad \text{.....Equation 2. 35}$$

The expression of the instantaneous contact radius is.

$$\left.\begin{aligned} r_1 &= R_{b1}\,tan\,\theta + S \\ r_2 &= R_{b2}\tan\theta - S. \end{aligned}\right] \quad \text{..... Equation 2. 36}$$

The term S in Eqs. (3.36) is the distance along the line of action between the contact point and original point. In the approach phase, S is negative and has a value of S_2. In the retreat phase, S is positive and has a value of S_1.

2.7 Thermal analysis

Thermal breakage is one of the main damage modes in plastic gears; therefore, it is important to simulate it accurately. For this reason, the gearing process was simulated using FEM. Frictional heat is calculated using data from the sliding speed and contact force, whereas hysteresis heat is calculated using the element stress results. The damage is evaluated using defined characteristic temperatures and comparing with the material properties. This topic will be discussed in the next section.

2.7.1 Temperature characteristics

The characteristic temperature is a temperature whose nature can be used as a reference for a real physical phenomenon. For example, the highest value of the surface temperature can characterize the phenomenon of galling, or the average value of the body temperature of the gear tooth can exist only on a purely conceptual level when identifying a mathematical concept.

The different characteristic temperatures encountered in a gear are as follows:

- The flash temperature: represents the highest value of the instantaneous temperature T_s surface on the contact width $2b$ of contact Hertz. The value depends on the equilibrium bulk temperature or T_s.
- The bulk temperature, T_{bi}: denotes the value of the temperature at all points of the tooth, as in the body on the surface in three dimensions. The integration of all local T_{bi} values at each point gives the average value of T_{bi}, often referred to as T_b and known by the name of "bulk temperature". The expression of the mean temperature from the local temperature values is as follows:

$$T_b = \frac{1}{N}\sum_{i=1}^{N} T_{bi}. \quad \text{.....Equation 2. 37}$$

Thus, in the case of plastic gears, a type of damage is caused by an excessively high temperature concentrated on the tooth surface, in this case, surface thermal damage. When the damage is due to general softening of the tooth, we say that there is generalized thermal breakage.

2.7.2 Friction heat

The displacement of the frictional force creates work, which is manifested by heating of the surface of the tooth and, in the long term, the entire tooth. The value of the heat of friction per unit time depends mainly on the friction force and slip speed, which vary with the mechanical or physical properties and parameters. The frictional heat generated at an interface is shared between the two teeth in contact, as will be discussed in the next sections.

2.7.3 Analysis of the heat production mechanism

From the beginning to the end of real contact, the amount of heat generated by sliding friction between two teeth is evaluated by integrating, over the course of the contact, the product:

$$dW = F_f V_s dt. \quad \text{..... Equation 2. 38}$$

This product represents the work of the frictional force during the interval of infinitesimal time dt. From the expression of the frictional heat for an infinitesimal time interval dt, this heat is directly related to that of the frictional force F_f.

F_f, the friction force occurring in the expression of the frictional heat, depends directly on the value of the distribution factor of the transmitted normal load, W_i/W. This factor is multiplied by the normal load, W_n, to yield the actual load, as previously discussed.

The distribution of W_i/W depends on the degree of contact extending out of the line of action, a phenomenon depending on the nature of the materials, the geometry and other parameters of operation.

In a spur gear, for a displacement ΔS of the contact point, the heat generated by friction for a unit face width can be expressed as

$$Eg_f = \mu W_0 \frac{W_i}{W} \frac{1}{\cos\theta_f} V_s \Delta S \quad \text{.....Equation 2. 39}$$

The max rise on surface contact temperature can be related to the frictional heat generated by the equating Archard's equation

$$\Delta T = \frac{E_{gf}}{4aK}. \quad \text{..... Equation 2. 40}$$

Where K, a are the thermal conductivity and the gear tooth width respectively.

2.7.4 The heat distribution factor

When the two teeth are in contact, the width of the contact surface 2b can be assumed to be thermally insulated for the contact time, and the instantaneous temperature is common to the two teeth.

It has already been shown that the instantaneous temperature at the contact point affects a thin layer on the contact surface; the thickness of this layer is smaller than the contact width 2b. When it is assumed that the temperature at the contact point for the two teeth is the same, the following expression of the heat distribution factor φ_2 is written for tooth 2

$$\varphi_2 = \frac{\sqrt{\rho_2 k_2 c_2 v_2}}{\sqrt{\rho_1 k_1 c_1 v_1}+\sqrt{\rho_2 k_2 c_2 v_2}} \quad \text{.....Equation 2. 41}$$

ρ_2 material density

k_2 thermal conductivity.

c_2 specific heat.

v_2 local instantaneous speed at constant point.

Calculating the value of φi at each position of the contact point requires the determination of a pair (V_1, V_2) of the local instantaneous speeds. These values must be calculated for the approach and withdrawal phases and for contact on the line of action and on the outside.

Heat is produced by friction from the surface of two teeth in contact. The study of the temperature rise experienced by a tooth requires quantification of the heat that affects one tooth at a time. For this purpose, a factor φ is determined when the total frictional heat is E_f. The multiplying factor to give the amount of heat recovery for one tooth is $\varphi_1 E_f$.

$$\left.\begin{aligned} E_{f1} &= \varphi_1 E_f \\ E_{f1} &= \varphi_2 E_f \end{aligned}\right] \quad \text{..... Equation 2. 42}$$

Where

$\varphi_1 + \varphi_2 = 1$

2.7.5 Block solution

As stated previously, it is not recommended to measure temperature close to loads. Many authors have used analytical equations and developed special methods to estimate the flash temperature. The solution of Block yields a simple formula for the maximum surface temperature increase under a Hertzian contact:

$$\theta_f = 1.11\mu W\left(\sqrt{V_1} - \sqrt{V_2}\right)(kpcw)^{-0.5} \quad \text{Equation 2. 43}$$

For an ambient temperature of 23 °c. a block solution for the maximum surface temperature is determined from measured temperatures at different load levels by Aljaz et al. as;

$$\theta_f = -8.46 + 16.7 * \sqrt{\sigma_f}\,(℃) \quad \text{Equation 2. 44}$$

σ_f = tooth root stress

Block's equation only gives the flash temperature elevation; the real peak temperature that can be used to identify the contact thermal damage is the sum of Block's equation plus the general tooth temperature.

2.7.6 Hysteresis heat

The hysteresis heat is due to the internal damping phenomenon present in plastic materials. Tooth deflections are small in metallic gears, and the effect of material hysteresis due to frequency variation is negligible. A polymer gear tooth deforms severely because of the low gear tooth stiffness. The material is heated when subjected to cyclic loading, such as is encountered in gears. When the amplitude of the stress to which volume element V of the tooth is submitted, Io, the loss of heat by hysteresis is expressed as

$$E_h = \frac{\sigma_0^2}{E}\frac{\pi}{2}\frac{tan\,\delta}{1+(tan\,\delta)^2} \quad \text{Equation 2. 45}$$

$\tan\delta$ loss factor

The deflection and stresses for each element were calculated in the quasi-static simulation; these values are used for the hysteresis heat calculation at every point.

2.8 Wear analysis

These wear forms occur because of the direction of the relative movement that occurs as the teeth enter and leave the mesh. Sliding is away from the pitch line on the driving gear and toward the

pitch line on the driven gear, giving rise to the particular wear pattern. A typical worn tooth profile consists of two scalloped wear zones, one starting from the tip and running to the pitch point and the other going from the pitch point to the root.

In addition to direct material loss, which leads to functional failure, wear of the surface causes the gear system to significantly modify its characteristics of vibration and noise. The mesh excitation is highly sensitive to the surface geometry. The wear surface affects the gear contact patterns such that the contact stresses and load distributions are changed to accelerate the appearance of other failure modes.

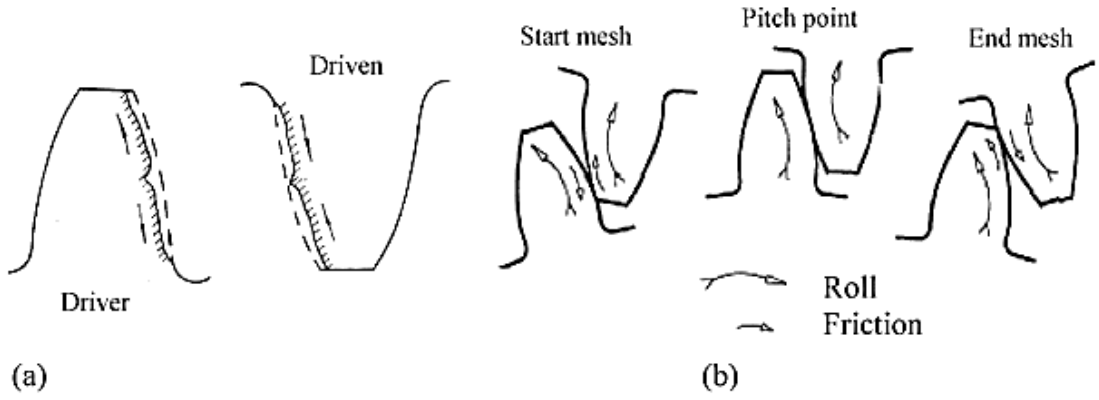

Figure 2. 5. (a) Gear surface wear forms and (b) gear rolling/sliding.

High-performance gears are generally lubricated with oil or grease. The state of lubrication is most likely in the boundary or mixed system, meaning that the lubricant film generated is not always sufficiently thick to separate the interacting surfaces. Sliding wear at point P on a dry contact or a mixed lubricated boundary surface can generally be regarded as a function of the initial value and described by a differential equation. The accumulated wear at a point P can be determined by Archard's wear equation

$$\frac{V_w}{S} = K_w \frac{W}{H} \quad \text{.....Equation 2. 46}$$

Where W is the applied normal load, V_w is the volume of the worn material, H is the hardness of the observed surface and K_w is the dimensionless wear coefficient. For a local area, the equation can be expressed as.

$$\frac{h}{S} = K_w p \quad \text{.....Equation 2. 47}$$

where h is the wear depth, s is the sliding distance where the point is sliding against the interacting surface, p is the local contact pressure, and k_w is the dimensional wear coefficient. The wear of point P on a rubbing surface with the wear model described by Archard equation is

$$h_p = \int_0^S kp\, ds. \quad \text{Equation 2. 48}$$

Although many researchers have proposed more advanced wear models using different methodologies and parameter sets, Archard's wear model remains the most commonly used model for practical applications, such as cam-follower contacts, engine piston rings, and gear contacts, where the geometry and operating conditions are already complex.

As previously discussed, the rapid increase in the wear rate as the maximum surface temperature or load increases is due to surface melting or the maximum Hertzian stress exceeding the yield point of the composite. At this point, we considered the gear to have failed.

2.9 Fatigue analysis

Gear teeth are subjected to alternate stresses at various points. This process can lead to failure by fatigue even if the elastic limit of the material is not exceeded. In particular, gears often break due to crack propagation in the tooth root.

2.9.1 Root fatigue

Standard procedures are available in the literature to determine the load capacity at the gear root. They compare the maximum tooth-root stress by a functional factor to the limits of the material. These standard procedures consider that only the gear hardness changes the fatigue life with the maximum tooth root stress.

When using data from normalized specimens, the values must be adjusted to consider the differences between the specimen and part. Some examples of differences to be considered in the specific case of gears are the particular shape, load application, size and operating temperatures. Coefficients that consider these factors are often called “fatigue reduction coefficients” and multiply the theoretical fatigue value to obtain the real value.

Additionally, these coefficients are often designed to be used with metal parts, and results using this methodology can be misleading without proper validation given the various particularities that distinguish plastic gear meshing from metal gear meshing. To obtain accountable results, we use

validated experimental data from the literature of gears having the size and material properties in the range of our model scope. This approach avoids errors induced by one or more inappropriate coefficients and enables estimation of the model interpolation error. The data modeling approach consists of approximating the number of cycles to root fatigue as a function of the bending stress/strength ratio plus a term that considers the effect of the rotational speed on the results. The proposed model is as follows;

$$Cycles_b = a_b R_{bss}^{b_b}(1 + c_b)^{1000-S_{rot}} \quad \ldots\ldots\ldots\ldots\ldots\ldots\ldots\ldots\ldots\ldots\ldots\ldots\ldots\ldots\ldots\ldots\ldots \text{ Equation 2. 49}$$

where the bending fatigue coefficients $a_b b_b c_b$ are $7.29E+2$, -3.33 and $2.65E-4$, respectively. R_{bss} is the bending stress at the root, and R_{rot} is the rotational speed in RPM.

2.9.2 *Contact* fatigue

Whenever two curved surfaces are in contact under a load, contact occurs along a line or point or, depending on the elastic constants of the materials concerned, along a small circular or elliptical area. As a result of such small contact areas, the shear (Hertzian) stresses that develop at and near the surface are extremely high.

Surfaces subjected to rolling and sliding contacts may suffer from contact fatigue; the mechanism causing rolling contact fatigue to initiate and propagate is not fully understood. There are a number of differences between classical fatigue and RCF that make it impossible to apply the results from classical fatigue to RCF directly.

The proposed model is as follows:

$$Cycles_c = a_c R_{css}^{b_c}(1 - C_c)^{1000-S_{rot}} \quad \ldots\ldots\ldots\ldots\ldots\ldots\ldots\ldots\ldots\ldots\ldots\ldots\ldots\ldots\ldots\ldots\ldots \text{ Equation 2. 50}$$

where the contact fatigue coefficients a_c, b_c, c_c are $9.59E{+}4$, -27.01 and $1.99E{-}03$, respectively. R_{css} is the contact stress at the root, and S_{rot} is the rotational speed in RPM.

Chapter Three

3. Simulation with Abaqus/CAE 6.14

3.1 Modeling of spur gear using Abaqus/CAE 6.14

The process of developing a simulation within Abaqus consists of eight steps, starting with model import and ending with job submission, as shown in Figure(3.6)below.

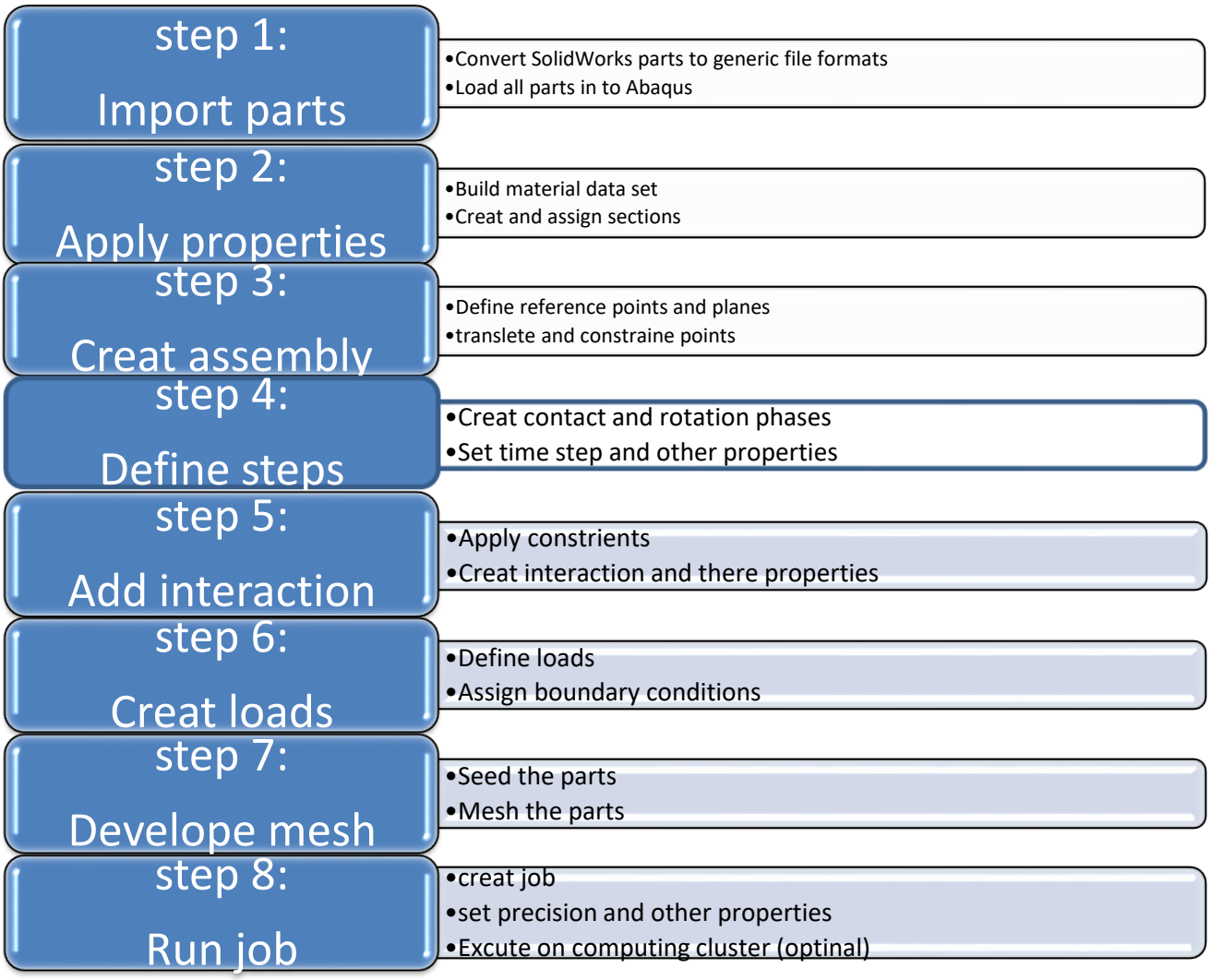

Figure 3. 1. Steps for developing a simulation with Abaqus/CAE 6.14

When using Abaqus, there are a number of options presented to the user regarding the type of simulation to be performed. The major choices are Abaqus/Standard or Abaqus/Explicit, which

support either a static or dynamic analysis. Generally speaking, a standard (or implicit) simulation solves unknown values at a specific time using the current system information to iterate and check for convergence. On the other hand, an explicit simulation solves unknown values from system information already known and does not require iteration or checking for convergence

3.1.1 Import Part

In order to bring the spur gear model developed in SolidWorks into the Abaqus environment, it must be converted from its proprietary SLDPRT format to another generic file type. This process poses certain challenges, which in the worst case results in the loss of geometric fidelity, and at best feature information. Therefore, the STEPAP 2014 format was chosen for its ability to preserve geometry, topology, colors, layers, geometric dimensioning/tolerance, and design intent.

To begin, with a new *Standard/Explicit Model Database* open, the *Import, Part* menu item can be used to bring in both the Driver and Driven Gears mentioned previously. The settings for this action can be left to their defaults, which will create an individual, 3D, deformable, and original scale model. When this is completed, the workspace will display one of the two gears (depending on import order) as seen below in Figure.

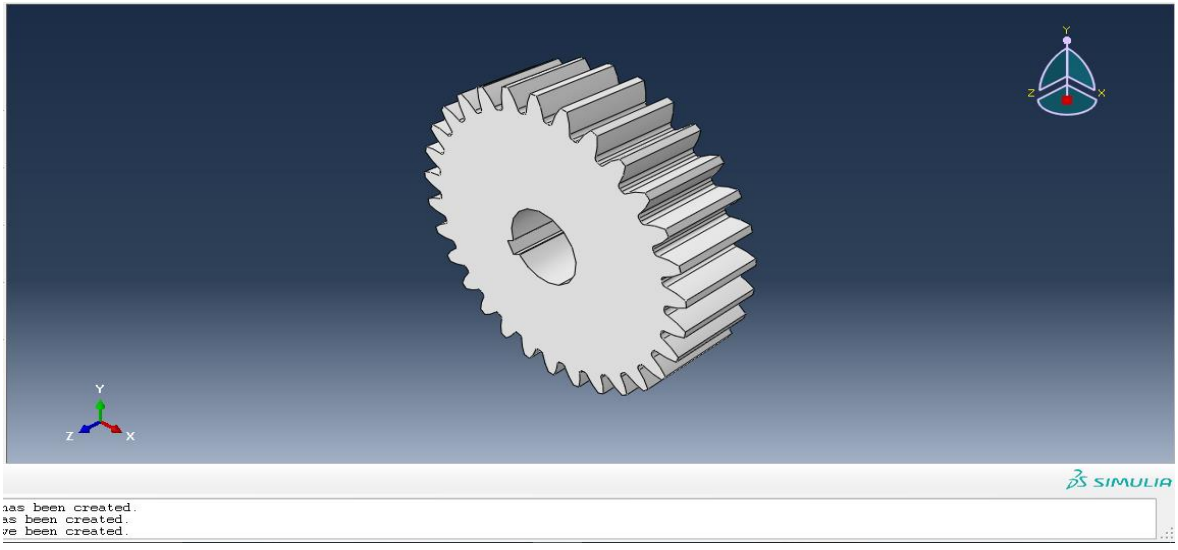

Figure 3. 2. Imported Part

3.1.2 Apply Properties

Next, the Module can be switched to Property, which will allow materials to be assigned on a part by part basis. Through the Create Material feature, it is necessary to assign density and

elastic properties. The specific values were set for the acetal nanocomposite as it was previously determined, taking or assuming the material to be homogeneous, with uniform elastic properties.

The issue of unit consistency is important to note since Abaqus does not have an inherent setting and once US or SI is selected at this stage, it must be used throughout the simulation. In addition, due to this flexibility, the units must agree with one another for accurate results (e.g. if density is in SI and elastic properties are US, the calculations will still take place despite being incorrect).Once available, *Create Section* can be chosen with the category and type set to *Solid* as well as *Homogeneous*, respectively. Then, using *Assign Section*, the previously defined properties can be added to both the driver and driven spur gears by switching between them through expanding the *Parts* category in the mod tree and selecting *Make Current* for the desired component.

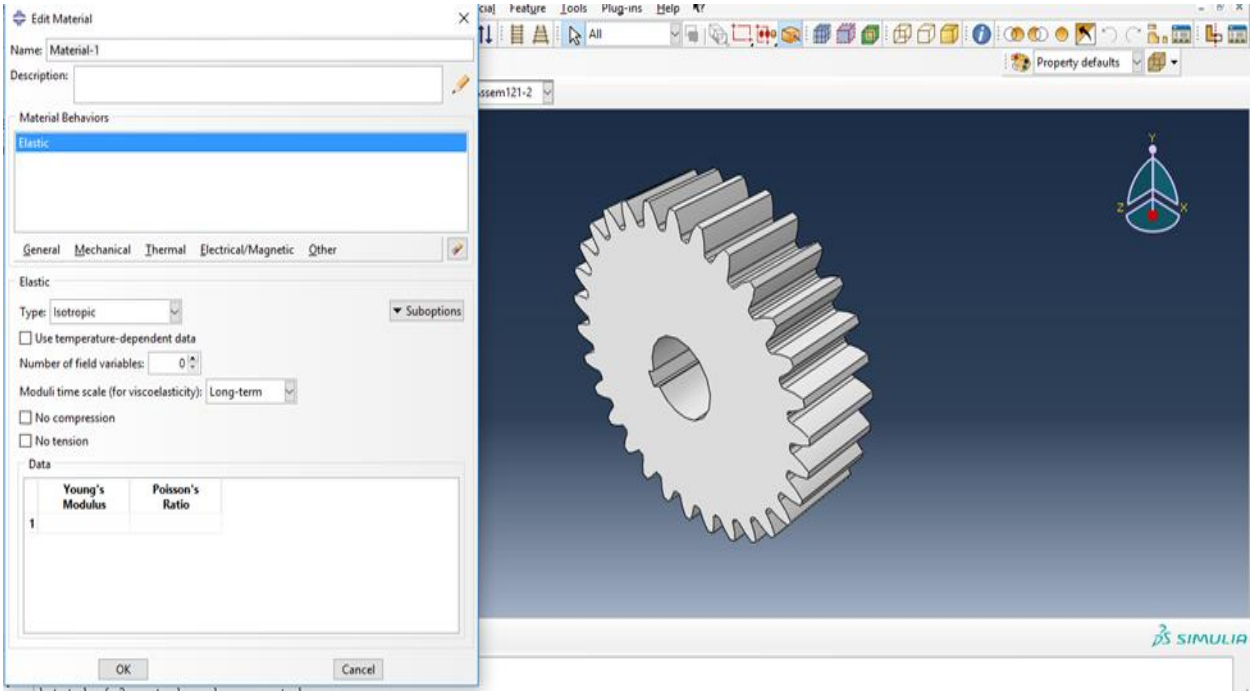

Figure 3. 3. Applying Properties

3.1.3 Create Assembly

Currently, both of the parts exist as separate entities, but if a successful simulation is to take place they must be brought together and their relationships defined. Therefore, once the module is switched to *Assembly*, both the driven and driver spur gear can be pulled in via the

create instance menu item and set to the *independent(mesh on* instance) type, after selecting parts and both parts as shown below.

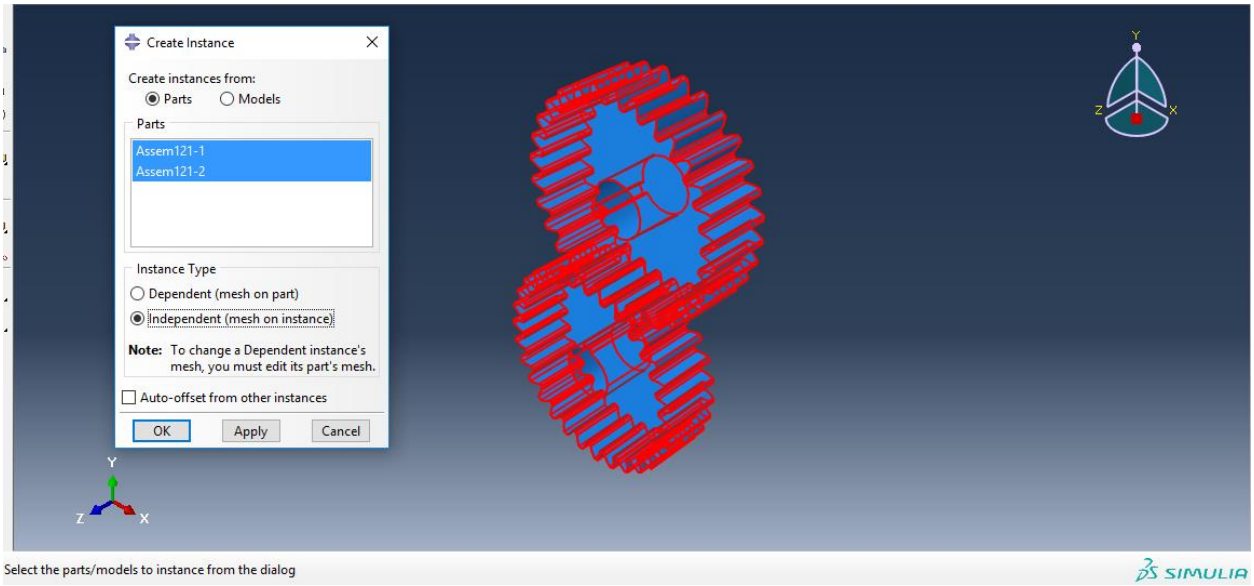

Figure 3. 4. Creating Assembly

3.1.4 Define Steps

When conducting a simulation in Abaqus, the process is composed of several distinct sections, or steps. Each of these provides the opportunity to define different boundary conditions (BCs), loads, constraints, and more in the Step module. This ability is integral to creating a realistic situation, and therefore accurate performance data. In this particular case, there are three steps defined from beginning to end: initial, contact, and rotation. The purpose of the initial step is to define the necessary BCs that will form the fundamental motion of the system. Then, the contact step ensures that the teeth of both the driven and driver gears meet and become a firm pair before full motion occurs. This is achieved by holding the driven gear in place and applying a specified torque to the driver spur gear. Lastly, the rotation step marks the beginning of the performance evaluation as the previous torque is held while a specified rotation is applied to the driver gear in the opposite direction. Each of these can be produced with the *Create Step* option and the procedure type set to *Dynamic/Explicit*. The *Incrementation* section should be the *Automatic* type, with the maximum number of increments set to 1000.

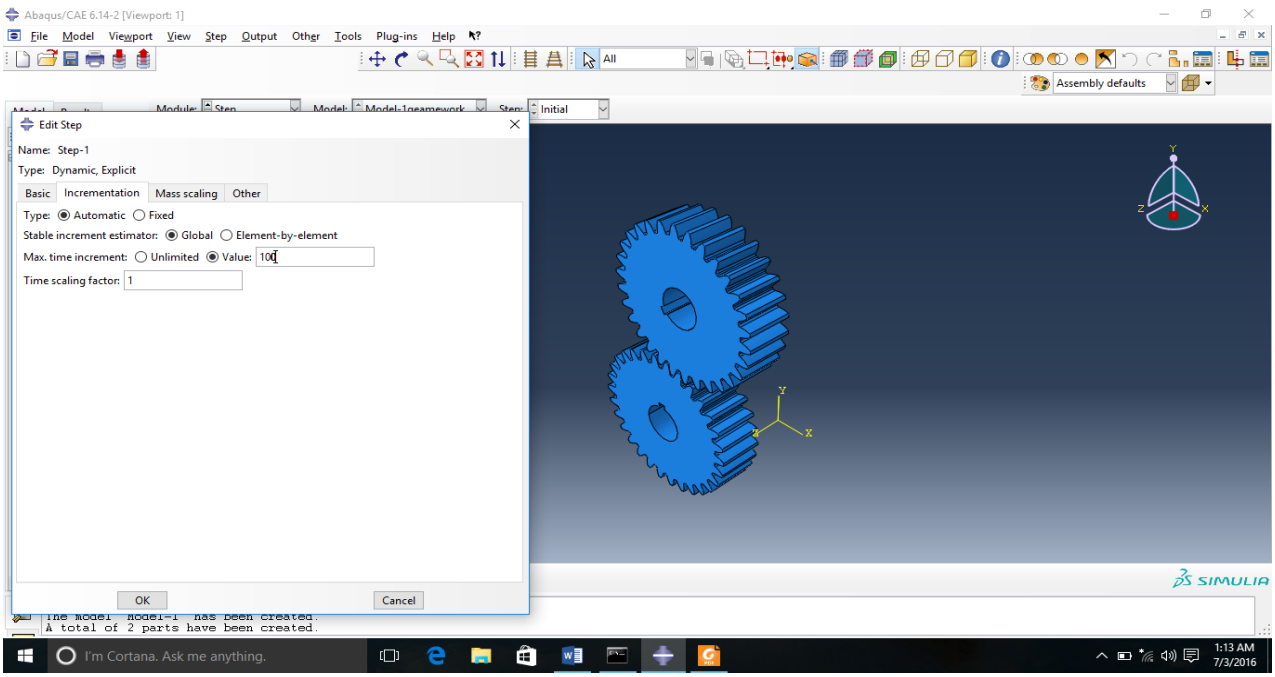

Figure 3. 5. Defining Steps

3.1.5 Add Interactions

The purpose of the *Interaction* module in Abaqus is to make the various models aware of each other, thus allowing realistic force and motion transfer to occur. The first step is to select *Create Interaction Property*, set the type to *Contact*, and then define both *Tangential Behavior* and *Normal Behavior*. The former can use the *Frictionless* formulation, whereas the latter should use *"Hard" Contact* pressure-overclosure. Next, in order to create the master and slave surfaces that are utilized by this setting, two groups must be created. The first, containing master surfaces, can be created under the *Tools* and *Surface* menu with the *Geometry* type setting. Now, it is necessary to select the two faces of every tooth present on either the driver or driven spur gear; either of these can be chosen first without consequence. The final task in ensuring the driver and driven gear perform as expected is to use the *Create Interaction* option to apply a global *Surface-to-surface contact (Standard)* starting on the contact step. Lastly, the *Contact Interaction Property* should be set to the appropriate parameters defined earlier which by default are contained in ''IntProp-1''.

Another aspect that needs to be considered is the spatial relationships of the two gears. they need to be fixed in space to avoid rigid body motion. Before this can be applied, however, *Reference Points* are required that are coincident with both the driven and driver gear datum points.

These can be added by the *Create Reference Point* option and selecting the datum points required. In addition, two new sets of geometry need to be assigned for use in the following step. By selecting *Tools* and *Set* in the menu, these can be assigned to the inner bore of both gears.

Once in place, these reference points and sets can be used with the *Create Constraint* option and *MPC Constraint* type. Specifically, the *MPC Control Point* is the reference point and the slave nodes are the bore set of either the driver or driven gear, respectively. Also, within this tool the MPC type should be set to *couple* to ensure the reference point and slave nodes share all displacements and rotations. This will ensure that any forces acting on the reference point will be effectively transferred to the gear body, allowing the simulation to take place. At this point, overall assembly of the system is complete, and will appear as shown in the figure below.

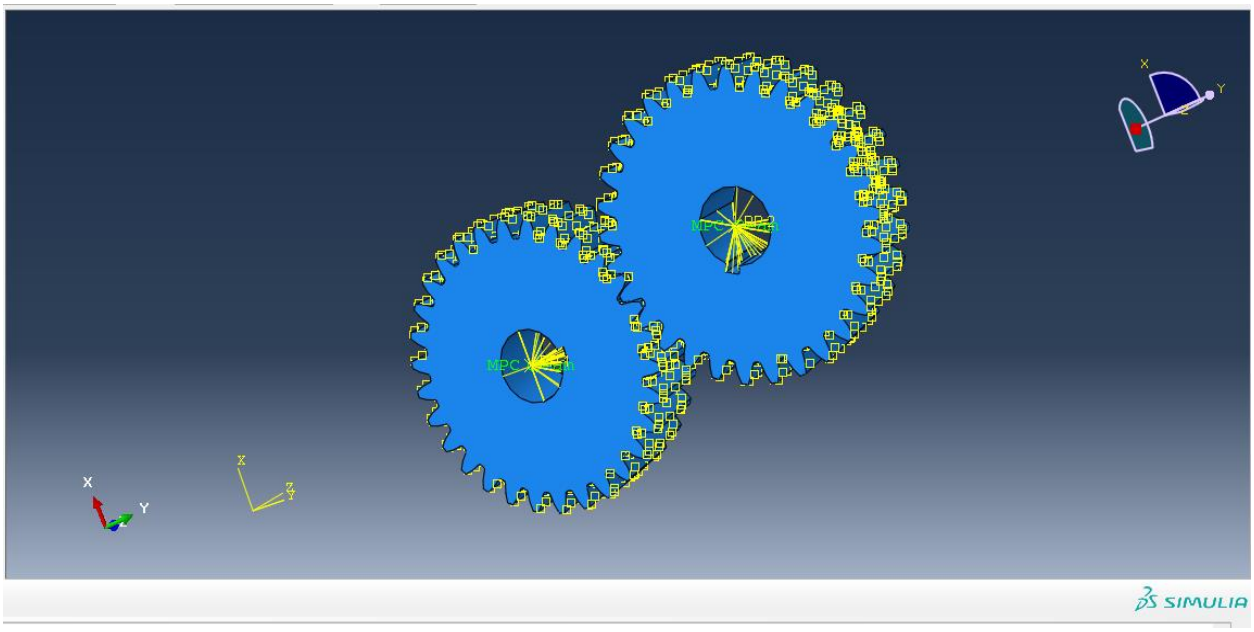

Figure 3. 6. Adding Interactions

3.1.6 Create Loads

The two primary tasks associated with the *Load* module are to apply loads and BCs to the previously created reference points. First, the *Create Load* option with the step set to *Contact*, category assigned to *Mechanical*, and type selection of *Moment* will provide the force needed to bring the two gears into contact. In this particular example, when prompted to decide on a location for the load, the *Sets* option should be used to select the driver gear reference point. This

type of assignment indicates that gear 2 will act as the driven part, whereas gear 1 will be the driver. Additionally, the load is selected from the previously performed experiment.

Next, the *Create Boundary Condition* option can be selected with the *Initial* step, *Mechanical* category, and *Displacement/Rotation* type. When prompted to select a region for the BC, the *Sets* option allows access to the previously created reference points. The first state of the system should be achieved by setting both the driver and driven to zero linear displacement as well as zero rotational displacement. However, since one gear can be considered the driven gear, it will be allowed to rotate in the Z-direction. Note that checking the box for a given direction indicates that value is fully constrained. Furthermore, it is important to make use of the alternative coordinate system created earlier for the external gear when assigning its particular boundary conditions. The X, Y, and Z constraints must be in this frame of reference due to the nutation angle, which modifies the way in which forces are resolved.

These particular BC and load settings will be propagated across all three steps created earlier, but where the *Rotation* step is concerned the BC on the external FG will need to be modified. This allows it to oppose the previously created torque load, and induce rotation in the system. For this modification, a specific angular displacement in the Z-direction should be chosen according to amount of simulation data required. In this case, a rotation totaling 2π radians was used due to computational considerations.

3.1.7 Develop Mesh

One of the key components of a successful simulation is an appropriate FE mesh. The practical considerations are as follows: assigning elements, seeding the parts, and meshing them. Before any of these can be addressed, it is necessary to set the object considered to part, rather than assembly, mode. This option can be found in the Abaqus toolbar, and is required because the the driver and driven gear were originally imported as dependent instances and must be modified on an individual basis. Once this change is made, a single part will be shown and the *Assign Element Type* option can be selected. This will allow the global settings to be adjusted, which should consist of *Quadratic*, *Tetrahedral* elements. This assignment should be applied to both gears using *Assign Mesh Controls* with the element shape set to *Tetrahedral*. An entity for these mesh controls will be requested, and the part of interest should be chosen. Next, the *Seed Part* option can be used; for the purposes of this study, an approximate global size of 0.06 was used in

combination with a maximum deviation factor of 0.1. In addition, the minimum size control as a fraction of global size was also equal to 0.1. Again, this procedure needs to be used for both parts. Lastly, selecting *Mesh Part* for both the driver and driven gear will complete this effort and result in an assembly ready for simulation. It was important to maximize the detail present on the tooth in order to achieve quality results, so that was balanced with computational cost in this case.

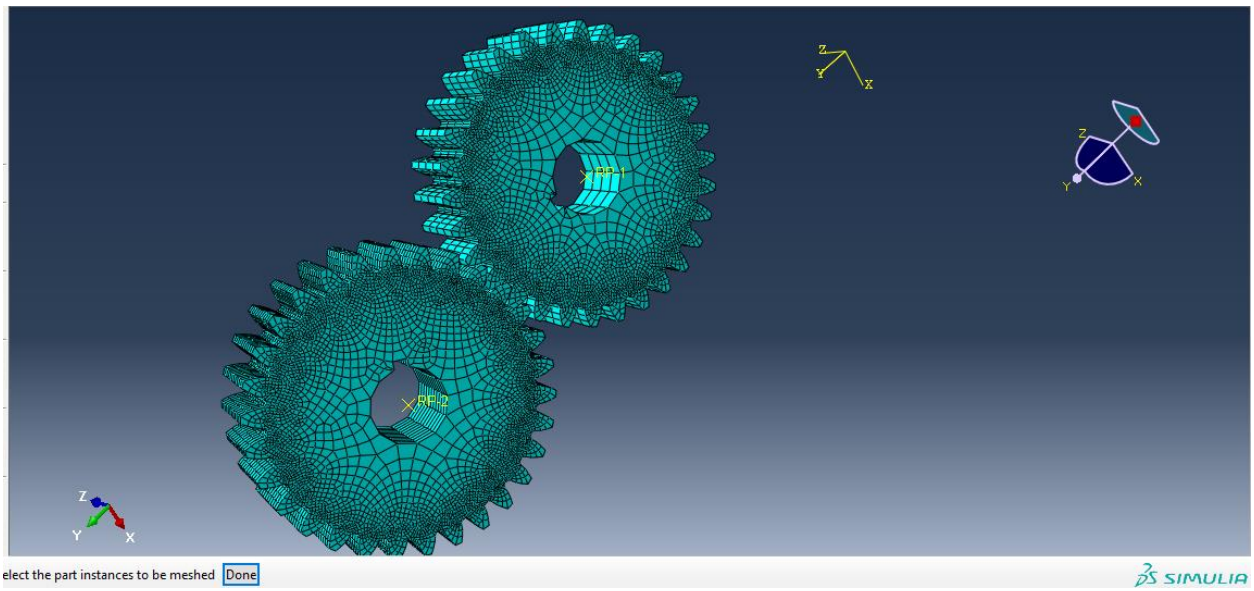

Figure 3. 7. Mesh developed

3.1.8 Run Job

The process for executing the simulation begins with the selection of *Create Job*, which will then provide a series of options under *Edit Job*. The majority of these can be left to their defaults, but a section of interest is *Precision*. The nodal output precision is typically set to *Single*, but for this case *Full* (or double precision) was used to ensure fidelity. Next, the *Job Manager* option can be used to *Submit* the job previously created. While this is running, the *Monitor* tool is useful to observe the current simulation progress and troubleshoot any warnings or errors. Note that warnings are fairly typical, especially concerning a limited number of distorted elements, and are non-fatal. It is up to the user to determine if these issues are serious enough to compromise the validity of the simulation, but with the settings described up to this point that is not the case. Finally, once complete, the *Results* tool allows the *Output Database* to be viewed and any relevant performance characteristics to be plotted and exported for further analysis.

Chapter four

4. Results and Discussion

4.1 Material property of the composite

The material property of the composite obtained from the previously suggested homogenization approach (*from equation 2.1 to 2.20*) is shown in the table below. MATLAB code is written to calculate this property. This newly obtained properties of the composite are used to perform FEM simulation using Abaqus/CAE.

Material	E(MPa)	Passion's ratio	Yield Strength(MPa)	Density(g/cm^3)	Thermal Conductivity (W/cm-K)
Acetal	1,400	0.35	79	1.41	0.0036
Silica	70,100	0.3	17000	2.2	0.014
Acetal nano-silica composite	3,780	0.32	108.7	1.74	0.0053

Table 4. 1. Material property of nano-silica reinforced acetal composite

As it can be seen from the above table the properties, thermal and mechanical, of acetal(polymer) has improved significantly by the addition of only 4.5% volume weight addition of nano-silica.

As it was clearly stated in the above chapters the objective of this study is to show that the overall performance of polymer gear can be enhanced by reinforcing it using nano particles. Results from Abaqus/CAE is used to analyze the nano composite gear wear, temperature resistance, and fatigue life, and the results are compared with the experimental data found from previous works.

In this paper Abaqus/CAE was initially used to analyze/simulate nanosilica reinforced acetal gear at a specific loading conditions mentioned on the previously performed experimental works by K. Mao et al., for pure acetal gear, and compare this results with the results obtained from the experiments.

4.2 Contour plot from Abaqus/CAE

Once the Abaqus simulation completes, an Output Database (ODB) file will be produced. This contains results for a range of parameters, including a visual representation of the system's motion. Initially, looking at the overall assembly, it is clear that there is a significant stress field being produced in the mesh during rotation. In Figure below, the results are shown, for a load of 8.5 Nm and running speed of 1000 rpm. This loading condition was found to be the maximum or critical loading condition that leads to failure for pure acetal gear by the experimental work conducted by K. Mao et.al. It can be seen that the teeth on the periphery of the mesh region are more lightly loaded than those at the center, and exhibit a clear point of contact. This stress propagates through the dedendum of the tooth and into the gear web, where the maximum value occurs.

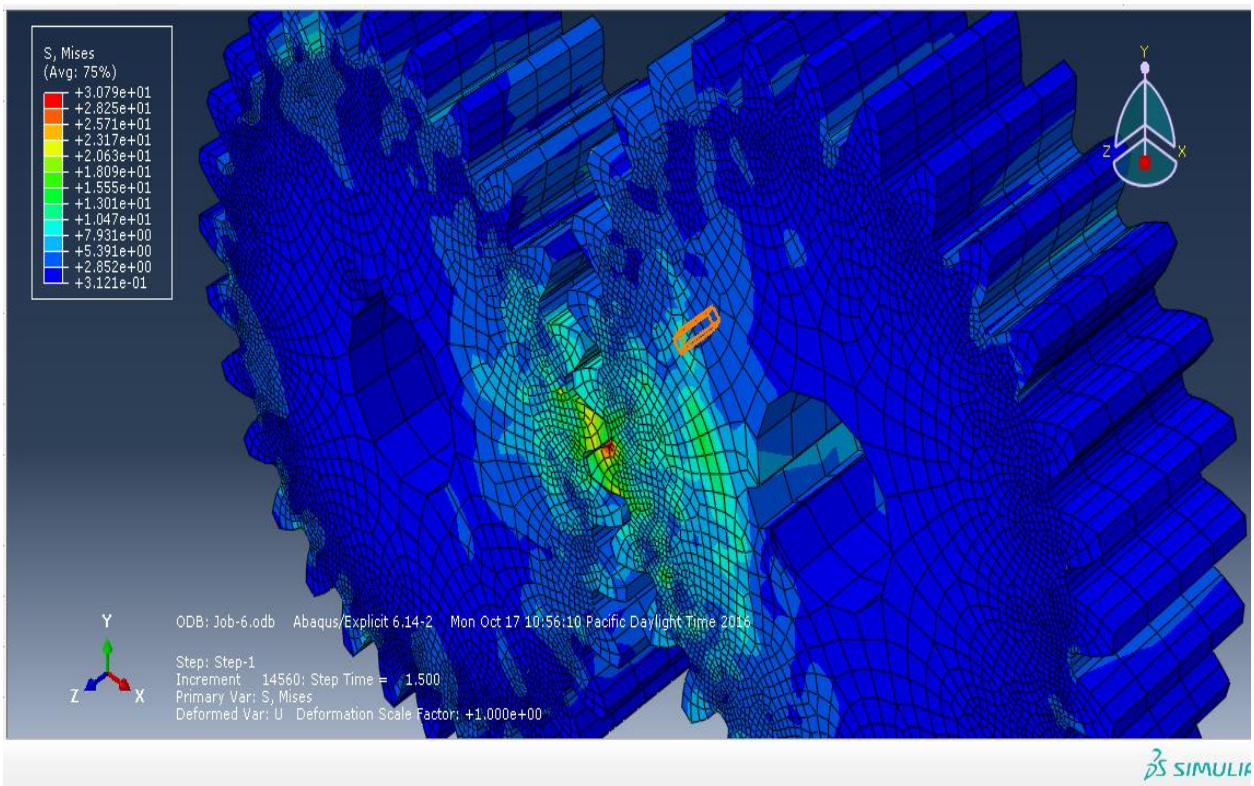

Figure 4. 1. Overall von Mises Stresses

By removing one of the gears (the driven) using the *Create Display Group* option, it is possible to examine these stresses at the same time step in detail. Looking at the driver in Figure there is a clear load concentration in this area, which increases towards the center of the mesh region. Also, it can be seen that the load is more uniform across the face of the tooth according to this trend as well. Overall, the von Mises stress reaches a maximum of **30.79 MPa** in this situation, which is generally acceptable for the material since this value is less than previously pridicted Yield strength of the composite. Taking the yelid yelid stength as the maximum allwoble stress this will give as a safety factor of **3.3** which is again acceptable for mechanical components.

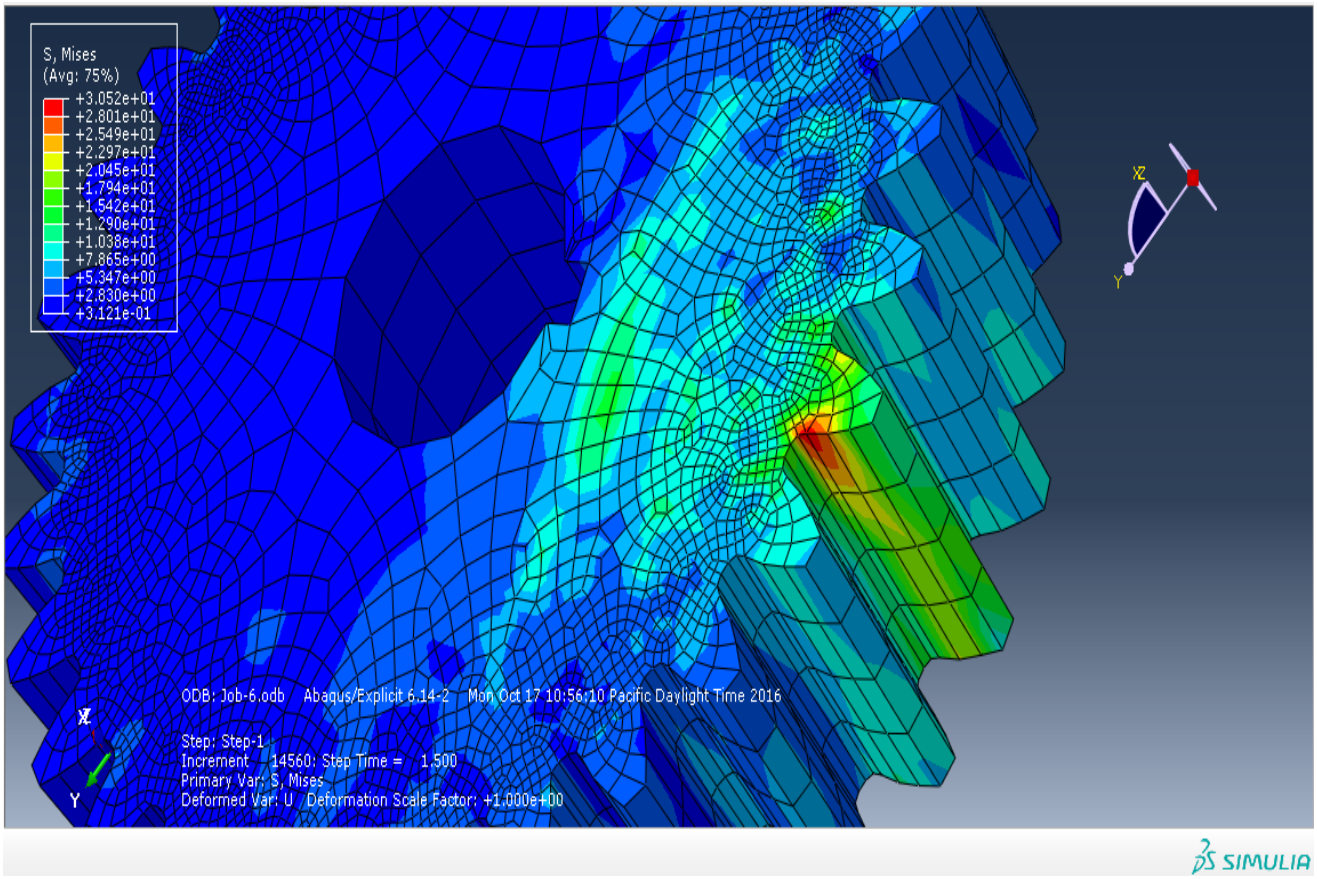

Figure 4. 2. Closeup of von Mises Stresses

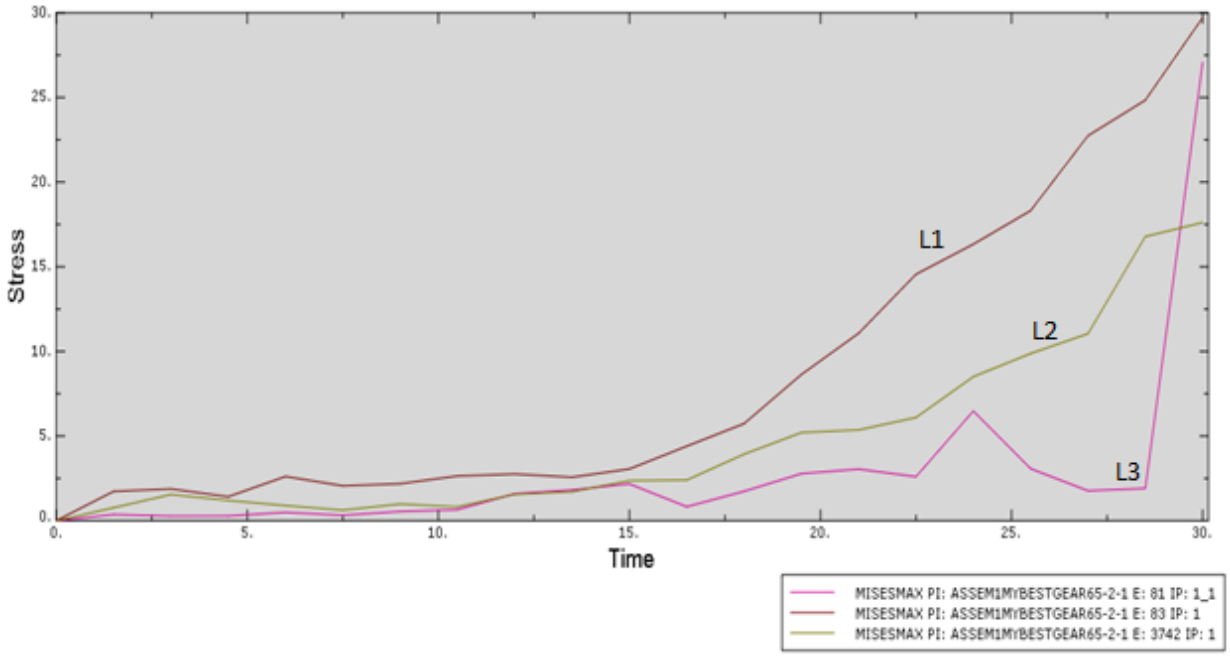

Figure 4. 3 Von-Mises stress distribution Vs time graph at different points of the gear

The above graph shows the Von-Mises stress distribution at different selected points on the simulated gear at 8.5 N.m torque. As it can be seen on the above graph the three lines represent the stress distribution at the root, the hub and at the middle of the gears surface. Line three represented by L3 shows the stress distribution or variation with time at the root, line two denoted by L2 is for a given point at the middle of the gear and L1 is for a given element at the hub of the gear. As it can be seen from the graph the stress distribution varies with time and for a given period of simulation the maximum values are seen at the root and the hub of the gear.

Another valuable metric to consider is contact pressure, which will help illustrate the interaction between the driver and driven composite gear. For the same part and time instant disscused priviosly the result can be seeen in the figure .this is further confirmation of the load distribution and mesh region charctestics disscused. In this case the pressure reaches a maximum of **26.03 MPa.** Note that tis interpritation apply equally for the driven gear too wich exhibites complimemtary behavioure to the driver gear shown here.

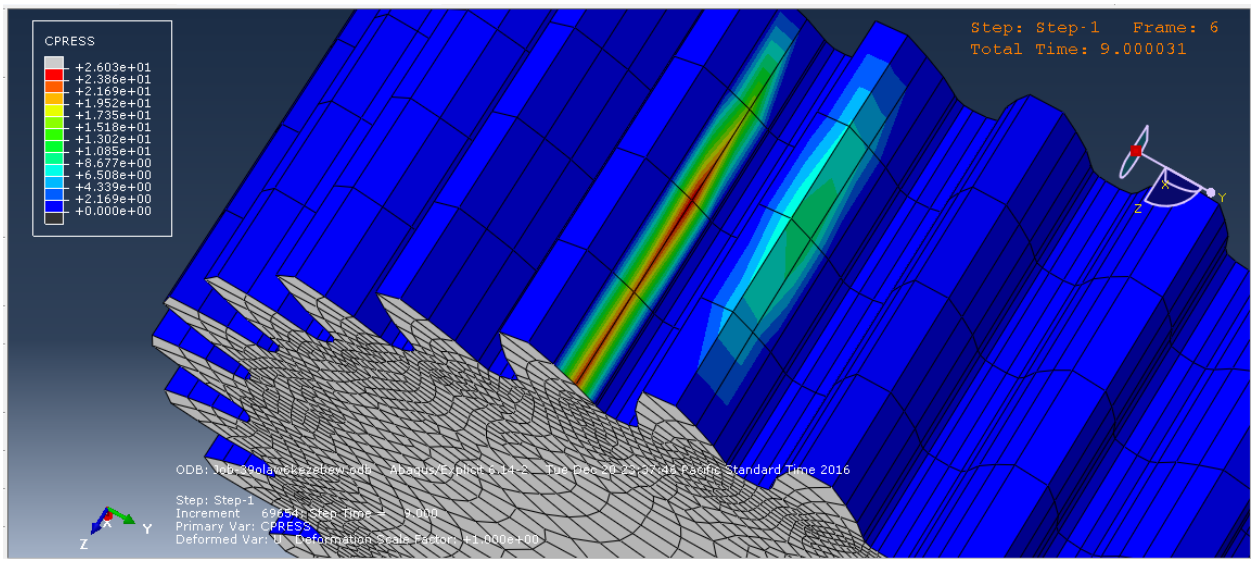

Figure 4. 4. Close-up of Contact Pressure

The results for maximum and minimum Von misses and contact pressure for different loading conditions is shown in the table below. This loading conditions are taken similar to the previously conduct experiment on pure acetal spur gear.

Load (N.m)	Von-misses stress (MPa)	Contact Pressure (MPa)
	Maximum	Maximum
6	22.19	10.95
6.5	22.98	13.90
7	24.63	14.18
7.5	26.05	20.05
8	28.14	24.21
8.5	30.79	26.03

Table 4. 2. Maximum Von-misses stress and contact pressure

4.3 Wear result and comparison with experimental data for pure acetal

According to the experimental work done on machine cut acetal gear by K. Mao et al. under a load of 8.5N.m, for 2.14* 10^6 cycles at a speed of 1000 rpm and, it can be seen that adhesive wear is the main wear failure mechanism for this machine cut acetal gear. This failure is expected as frictional heat is the main thermal source and the highest sliding friction contacts are located in the

addendum and dedendum regions on the gear surface. Similar conclusions can be made from the contour plot result found from Abaqus/CAE simulation. As it can be seen the stress concentration is high around the addendum and dedendum region, which is the main cause for the increment of surface temperature around this region's leading to higher wear rates around this parts of the gear.

Again looking at the Abaqus/CAE contour plot for the contact pressure we can observe that the maximum contact pressure values are found above the pitch point around the tip region and below the pitch point. This result also coincides with the wear patter observed on the experimental work which was mention previously and shown in the figure below. This shows that the simulation results are similar to the experimental result as compared to the wear point.

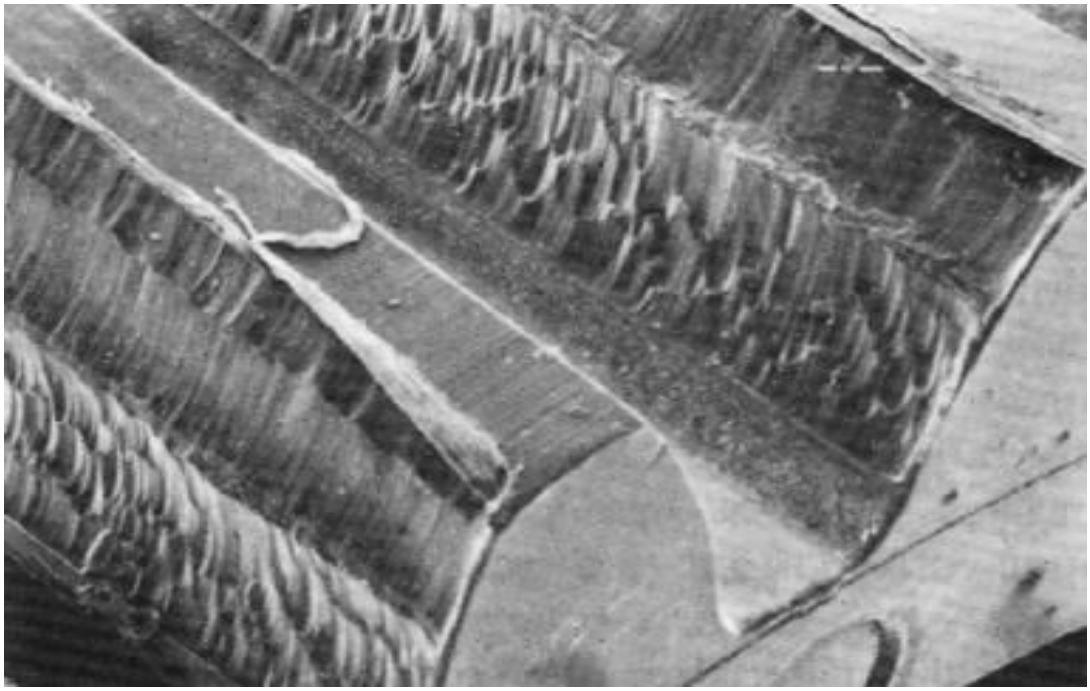

Figure 4. 5. SEM of acetal gear wear

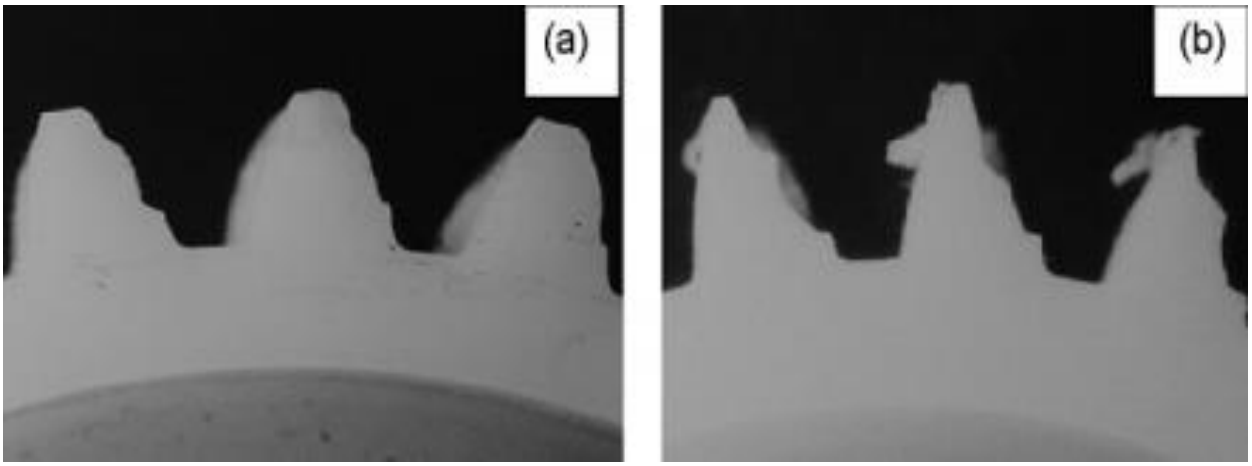

Figure 4. 6. Acetal gear wear forms under loads of (a) 7 Nm, (b) 10 Nm

Using the result from Abaqus which is the contact pressure the analytical approach suggested by equation (3.47) the wear depth is predicted and this value is compared with the wear depth value obtained from previously performed experiment by K. Mao et al. for pure acetal gear. The results for different loading conditions ranging from 6Nm to 8.5Nm are shown in the graph below.

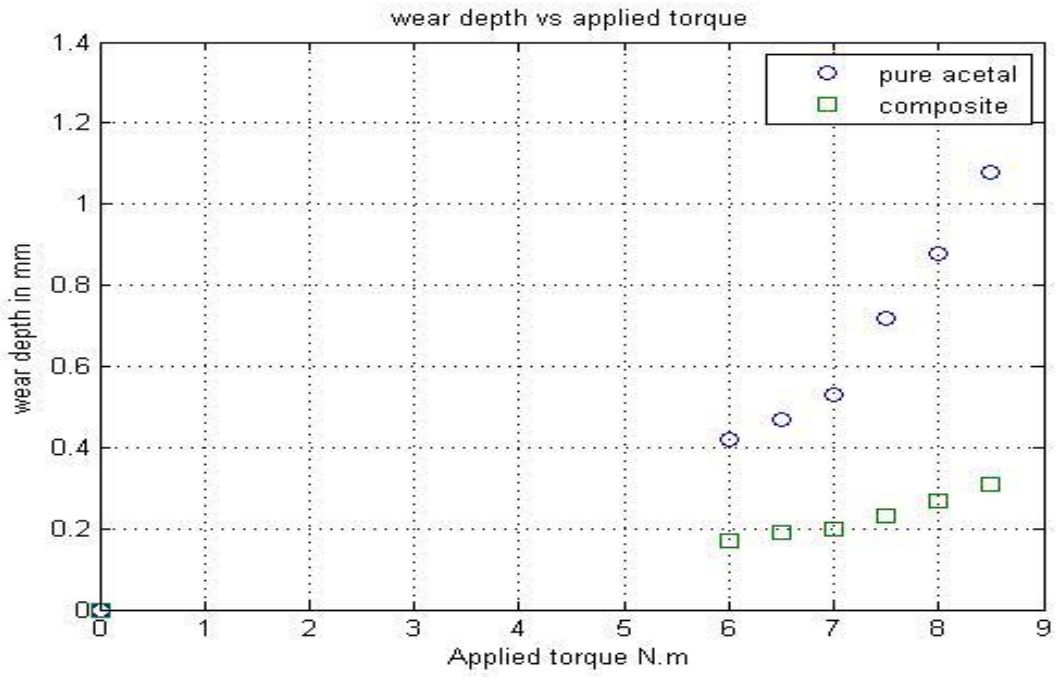

Figure 4. 7. Torque VS wear depth graph for pure acetal and nano-reinforced acetal gear

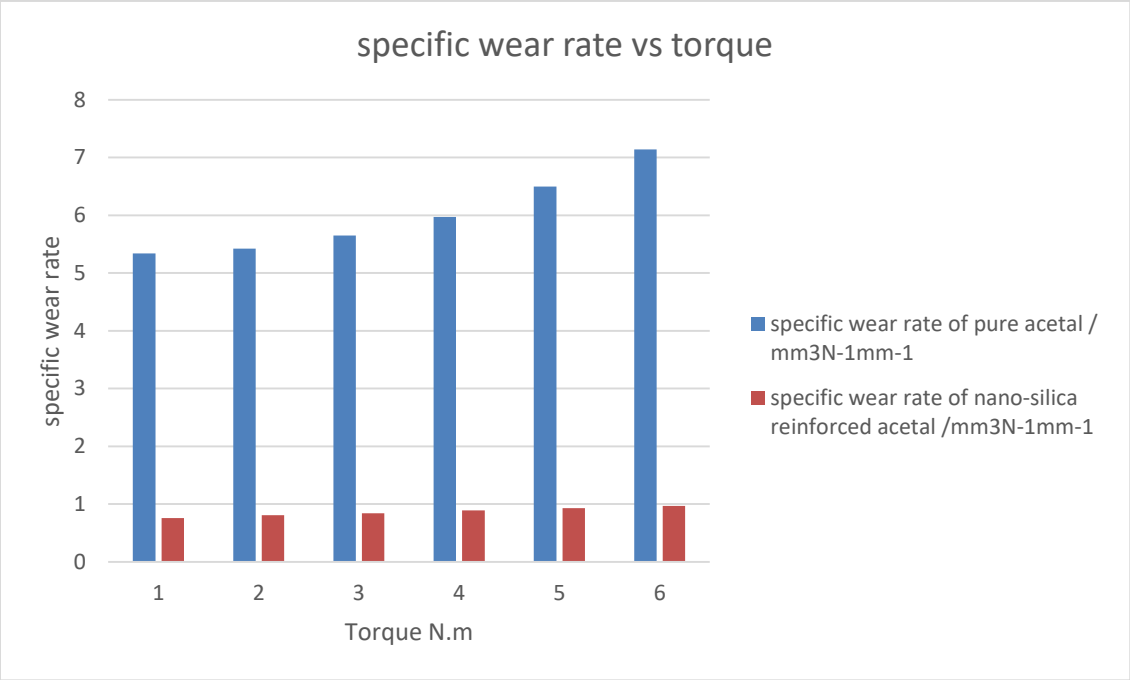

Figure 4. 8. Specific wear rate ($mm^3N^{-1}mm^{-1}$) for pure acetal and nano-reinforced acetal gear

As it can be seen from the above graph and also proven on the experiment by K. Mao et al. the wear rate of pure acetal increases rapidly when the gear is loaded above its critical load that is 8.2Nm. But the specific wear rate for nano-reinforced acetal gear is almost constant for the load range specified previously. Looking at the two graphs it can be observed that the wear resistance of acetal gear has increased by 300 %, by the addition of 4.5% weight volume of nano-silica in the matrix.

According to the experiment conducted for pure acetal gear, after gross wear (nearly 33% of tooth thickness), the gears eventually failed in thermal bending. This gross deformation is not always a plain fracture but is caused by high loads giving rise to softening of the acetal. The gear teeth are, probably, momentarily melted and as a result the teeth jump out of mesh. Which proofs the suggestions made by different literature that the main cause for the failure is low temperature resistance of the material which is polymer.

4.4 Surface temperature prediction

As it is mentioned on the literature review the temperature rise at the gear tooth is the main cause of failure for polymer gears. As it is shown by the works of K. Mao et al. for acetal gear and

supported by different literatures the maximum surface temperature of a gear is made up of three components, the ambient temperature of the surrounding, the bulk temperature, rise of the gear temperature above the ambient temperature and shot duration flash temperature rise where the gears mesh. Using the energy approach suggested by equation (3.40) and using the data obtained from Abaqus/CAE that is heat energy due to friction, the flash temperature is predicted for different loading conditions. In the energy approach it is assumed that there is no hysteresis heat loss. And the bulk temperature approach suggested on equation (3.44), using the stress values obtained from Abaqus/CAE, the bulk temperature is predicted.

Load (Nm)	Frictional Heat Energy (W)	Flash temperature due to friction (℃)	Modified Blok temperature (℃)
6	0.216	60.2	71.57
6.5	0.276	64.4	76.13
7	0.28	66.3	79.67
7.5	0.32	69.8	80.28
8	0.35	72.4	81.93
8.5	0.4	74.6	82.8

Table 4. 3. Gear tooth surface temperature at different loading conditions

As it can be seen from the above table the surface temprature results obtained using the energy approch is lower than the Blok temprature or the modified approch. As it was mentioned and proved by different experimental works determing the surface temprature of the gear tooth is on of the main chalenges of polymer gear design. The modifed bloks approch was proven to correlate well for limited number of teeth, incluyding the one in this reserch and at ambinet temprature of 23℃.

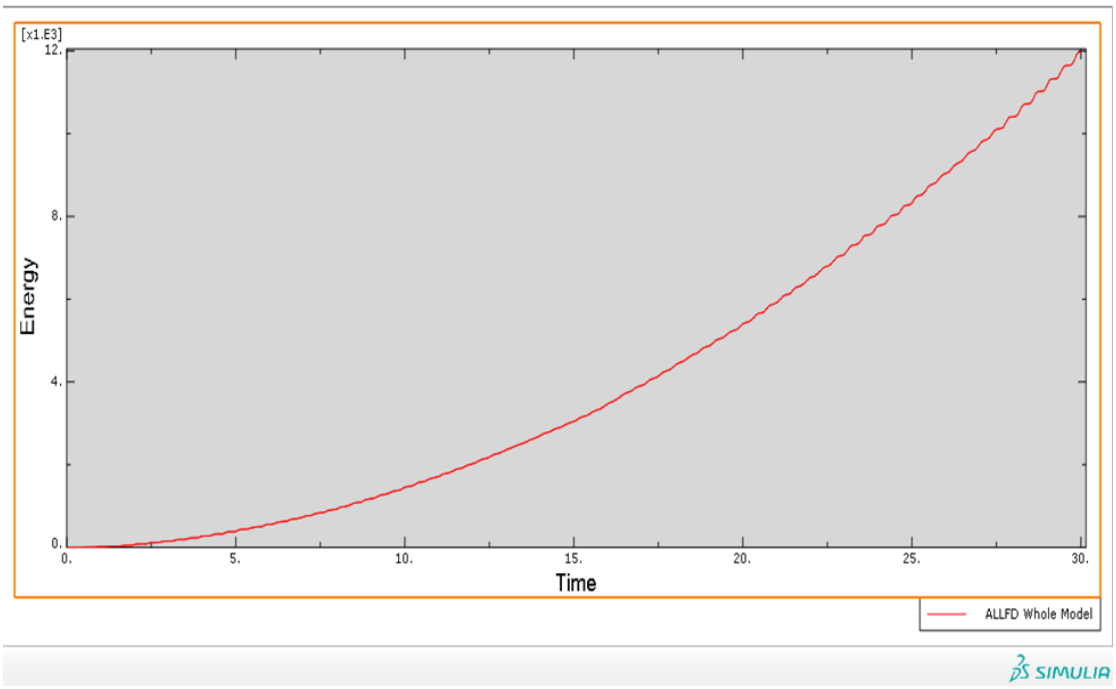

Figure 4. 9. Frictional energy dissipated vs time for a load of 8.5 Nm

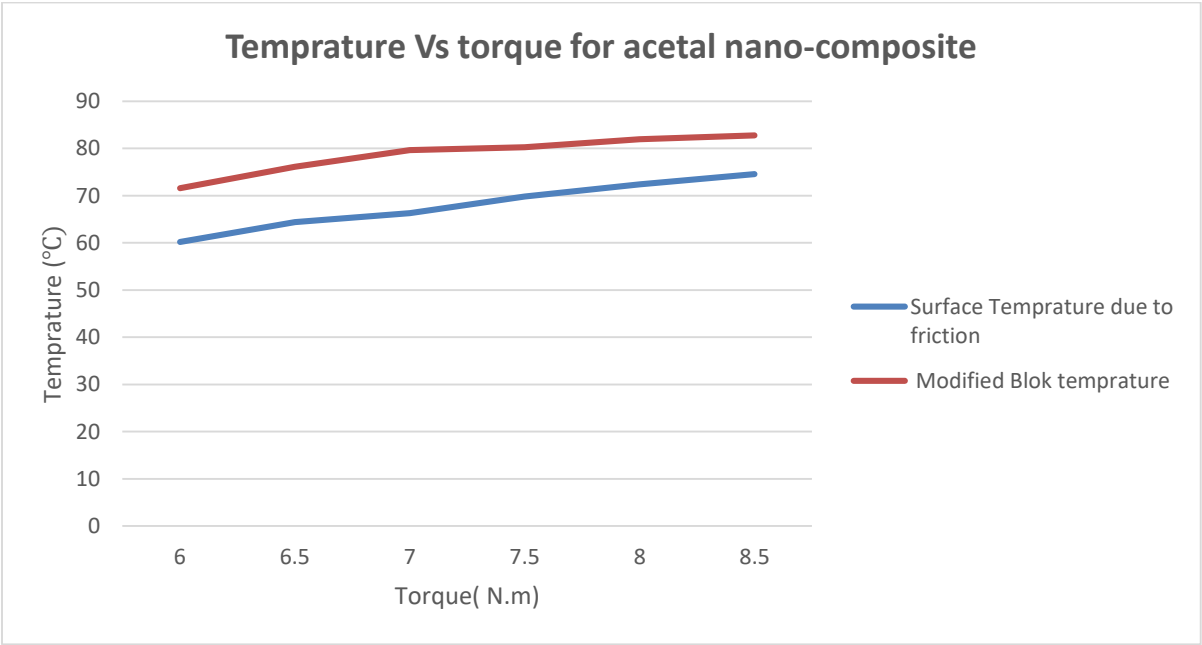

Figure 4. 10. Gear surface temperature Vs torque plot for acetal nano-silica composite gear

As it was found by the experimental work of K. Mao. et al. the melting point temperature of pure acetal gear is 165℃ and this temperature is reached at a load of 8.5N.m, 1000rev/min. The same loading conditions suggested for acetal gear on the previously mentioned experimental work are applied on Abaqus simulation software and the obtained results are shown on the graph above. As it is shown above from the obtained result for nano-silica reinforced acetal gear exhibits a much better temperature resistance than pure acetal gear. At the critical load mentioned on the experiment previously discussed the melting point temperature is reached at a load of 8.5 Nm but the surface temperature of nano-reinforced acetal gear at the same load is 82.8 ℃.

Applying the critical and ambient temperatures to the model on Abaqus/CAE the maximum von misses stress was found to be **38.78 MPa,** which again is less than the yield strength. Which shows that the newly proposed composite gear is capable of working at a higher temperature than pure acetal gear.

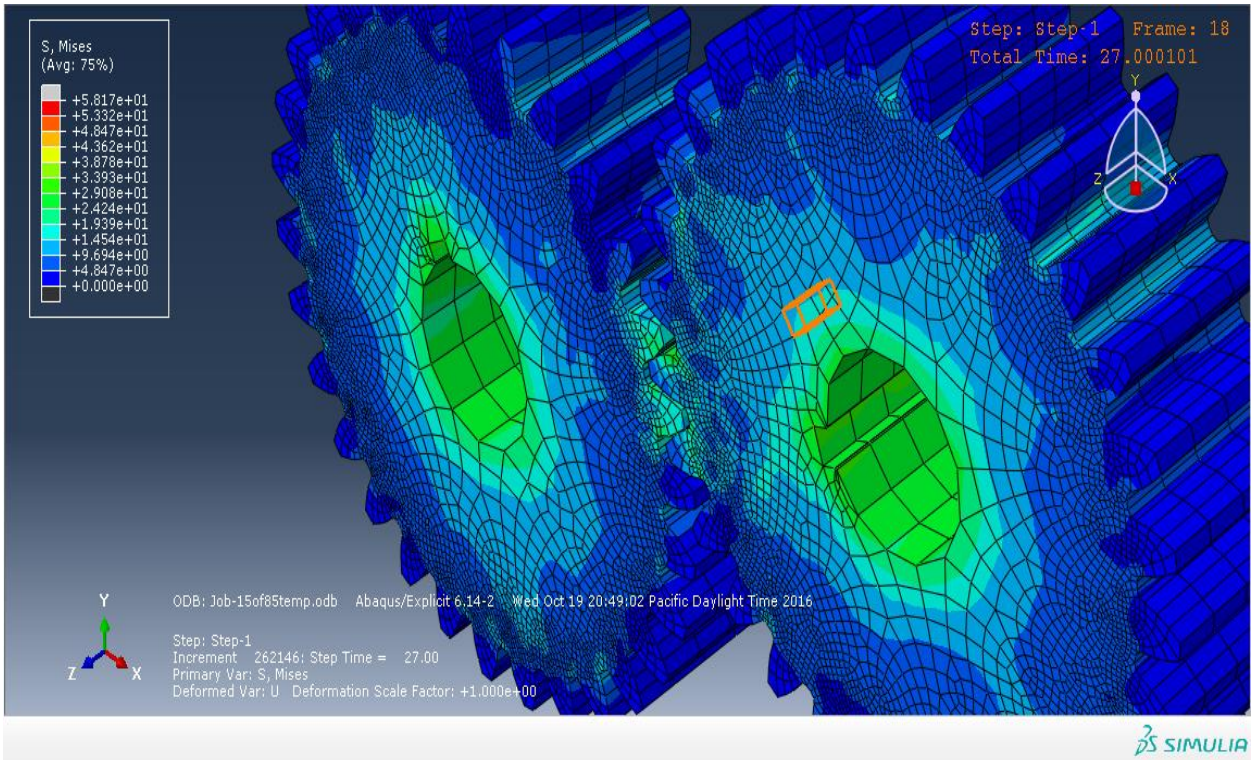

Figure 4. 11. Contour Plot for Von-misses stress at a load of 8.5Nm ,1000rpm and 165℃

This could be due to the overall improvement in mechanical and as well as thermal property. As it is given by equation (18) and (19) the thermal conductivity of nano reinforced acetal gear has increased by 47%, compared to pure acetal. And the surface temperature of this composite gear has decreased by 50% as compared to pure acetal gear.

4.5 Fatigue analysis

The suggested material stability is also checked for plastic deformation by the aid of the stress-strain curve obtained from the Abaqus/CAE 6.14. The stress-strain curve for different positions/locations of the gear are shown below.

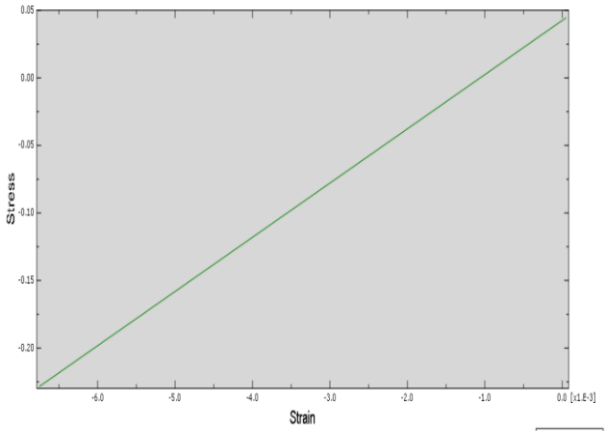

(a). Stress(11) vs strain at the tooth tip.

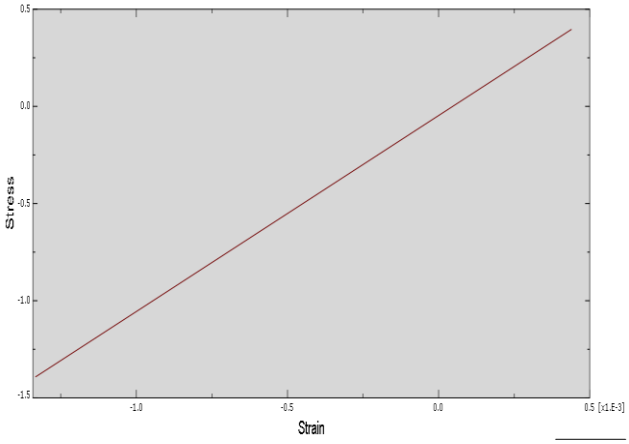

(b). Stress (12) vs strain at the root tip

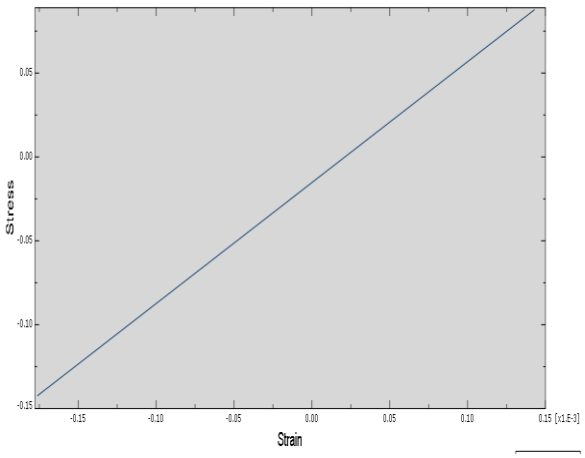

(c). Stress(13) vs strain at the tooth tip.

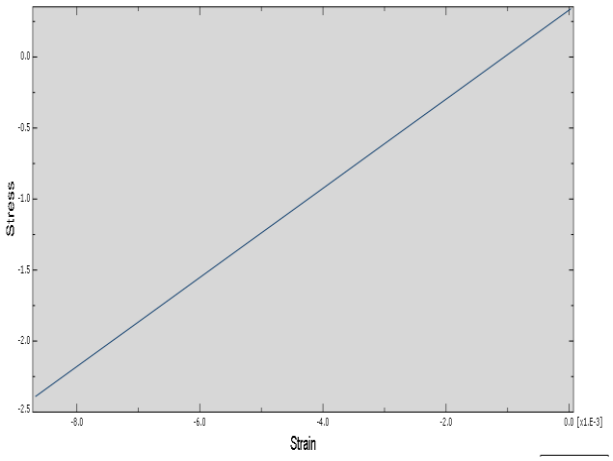

(d). Stress (22) vs strain at the root tip

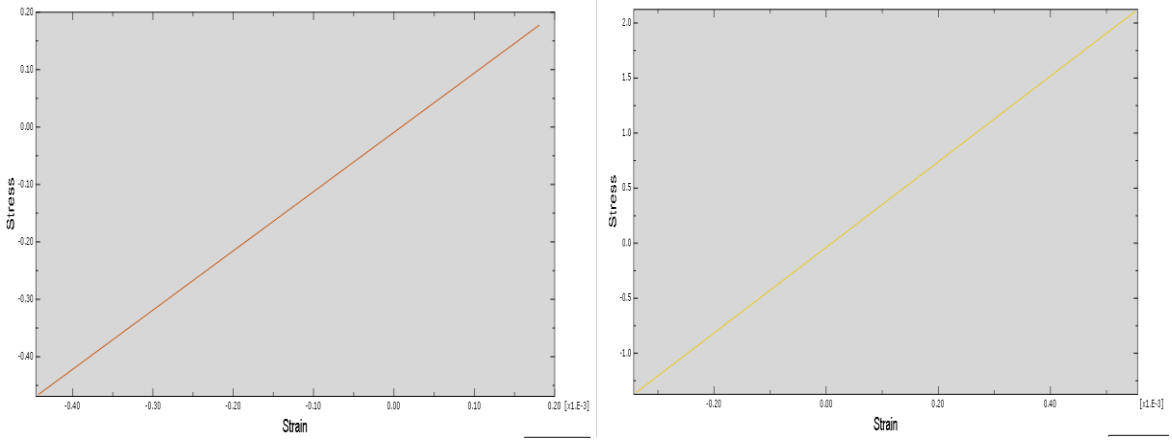

(e). Stress (23) vs strain at the tooth tip (f). stress (33) vs strain at the tooth tip

Figure 4. 12 Stress vs nominal strain plots for acetal nano-silica composite gear at the tooth tip

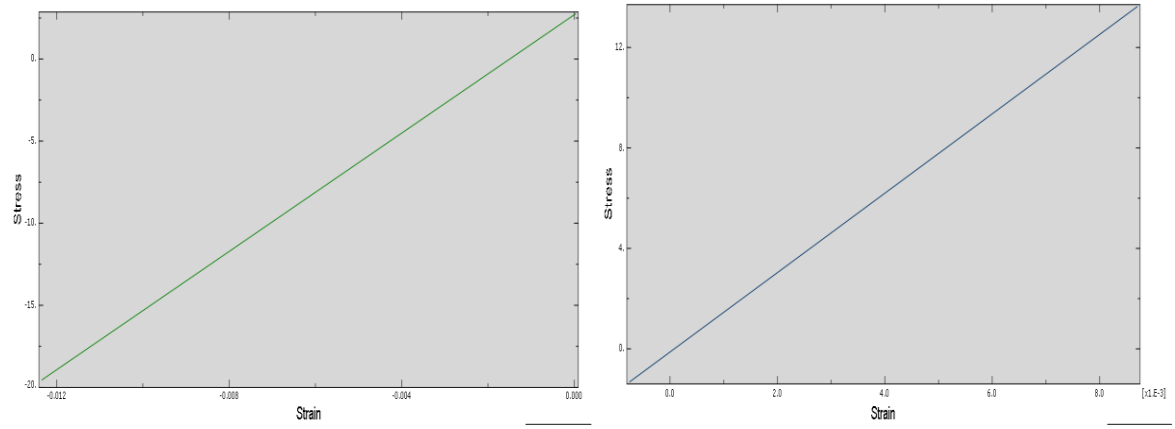

(a). Stress (11) vs strain at the tooth root (b). Stress (12) vs strain at the root

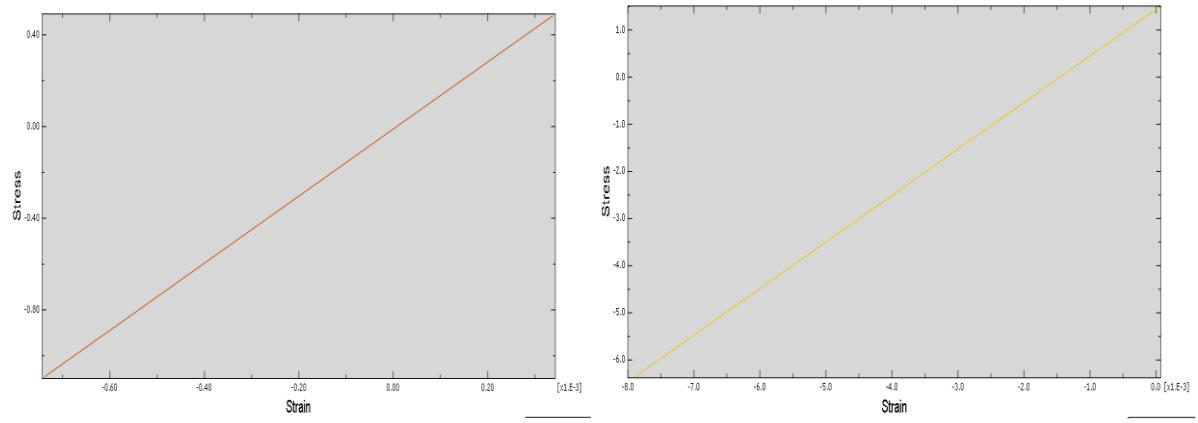

(c). Stress (13) vs strain at the root (d). Stress (22) vs strain at the root

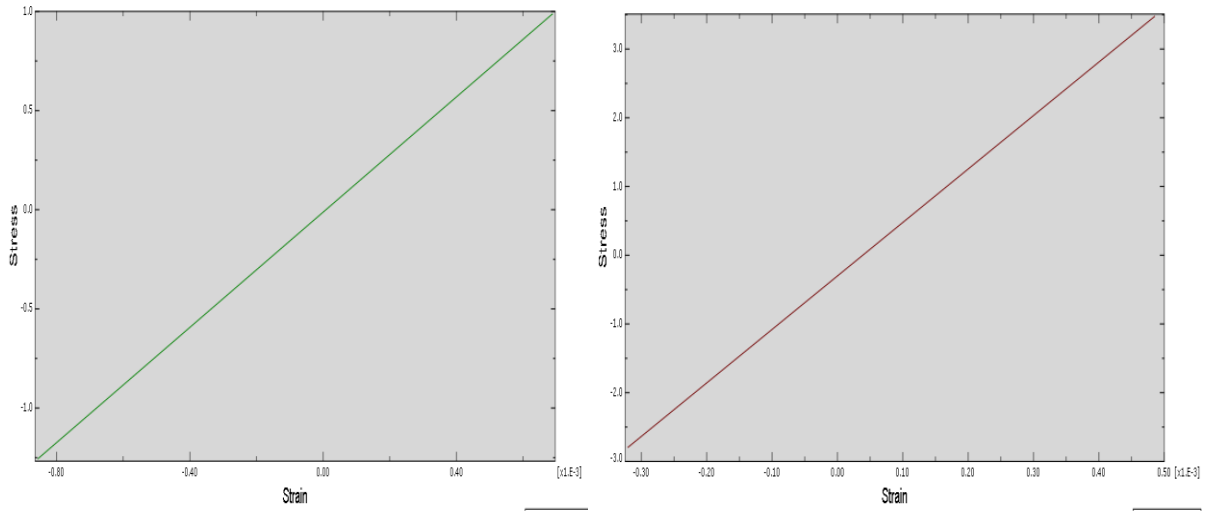

(e). Stress (23) vs strain at the root (f). Stress (33) vs strain at the root

Figure 4. 13 Stress vs nominal strain plots for acetal nano-silica composite gear at the tooth root

It should be noted that the end point of the curves indicates, how far this simulation was conducted and hence should not be taken as the yield point of the suggested material and this is due to Abaqus/CAE *Dynamic/Explicit*, simulation needs a large computer space and a considerable or large time to simulate. As it was previously discussed and shown on the graph clearly the stress values are much less than the yield strength of the composite predicted earlier. Under the same loading condition, the stress-strain graph for pure acetal gear is also given. Since the maximum stress therefore also strain is found to be at the root of the gear tooth the plots represent the values for this region.

From the above plots it can be seen that for the period of performed simulation the composite remains in the linear elastic zone, without any transition to plastic zone, which again assures the composites ability to carry or run under the proposed load. As it can be observed on the above plot the maximum stress is found to be at the root of the tooth, with maximum **tensile stress 12.4 MPa** in the **XY plane**(direction) and maximum compression stress of **6.3 MPa** in the **Y** direction. Another very important observation that can be made about this composite from the stress strain curve is that, the area under the stress strain curve that represents the toughness has increased, as

compared to the stress strain curve expected from polymers (acetal) which shows larger strain rate for a small stress.

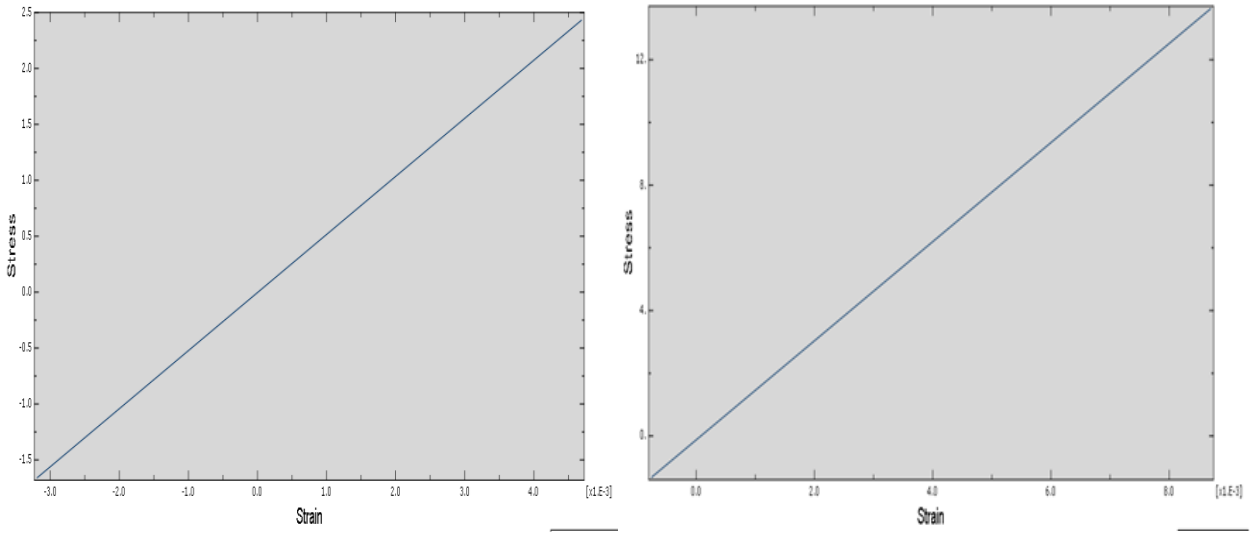

(a) *(b)*

Figure 4. 14 (a). Stress vs nominal strain plots for pure acetal gear at the toot root (b). Stress vs nominal strain plots for acetal nano-silica composite gear at the tooth root

If we compare the results for the acetal composite shown at the previous graphs with the one obtained for pure acetal shown above, for the same value of stress the strain rate is larger, or there is a larger amount of stress for a very small strain, indicating that the toughness of the polymer is increased, and looking at the shape of the graph it can be concluded that the, the composite still possess ductile property. Taking the area under the curve for both the pure acetal and the nano reinforced one it can be seen that the toughness of the polymer composite is approximately 10 times more than the pure acetal.

Different models suggest different approaches taken from experimental data but the one selected to analyze the fatigue life and time of failure due to fatigue of this nano reinforced polymer gear as shown in equation (49) and (50). The fatigue analysis is done for two types of fatigue failures as previously mentioned. The tooth root fatigue analysis given on equation (49) and contact fatigue

given on equation (50). The values for that used in the equations which are the root bending stress and root contact stress are obtained from Abaqus/CAE simulation results.

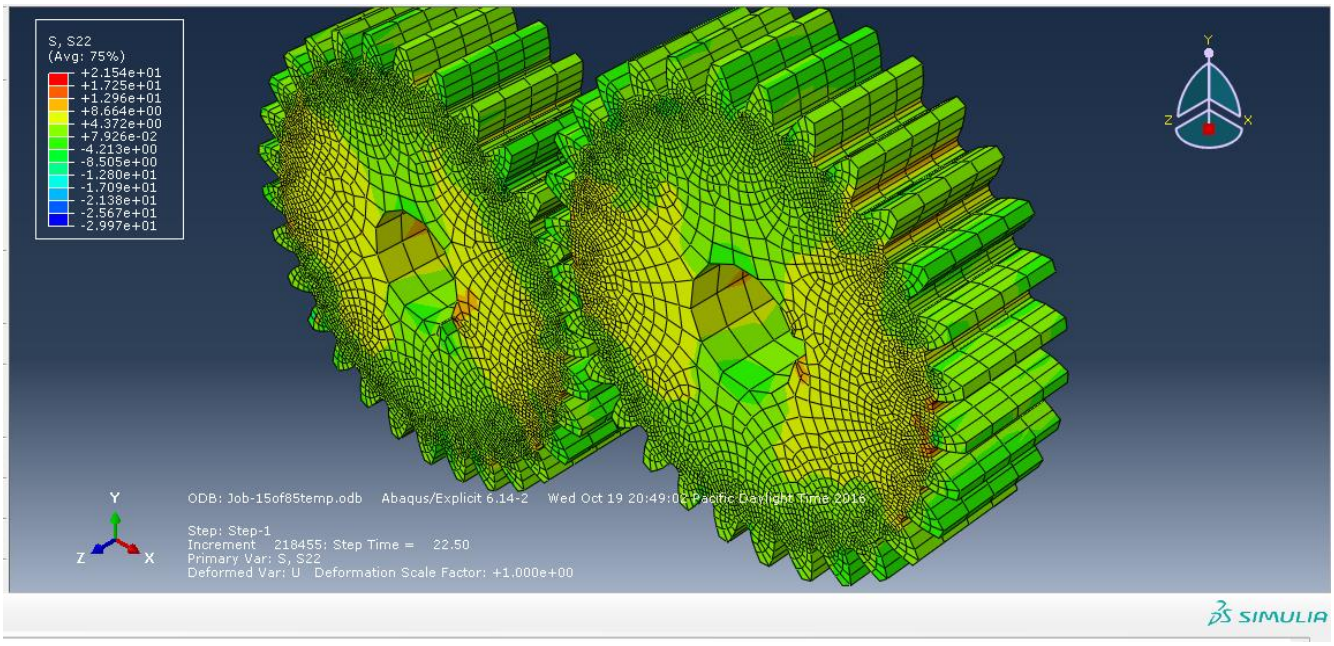

Figure 4. 15. Contour Plot for Bending stress

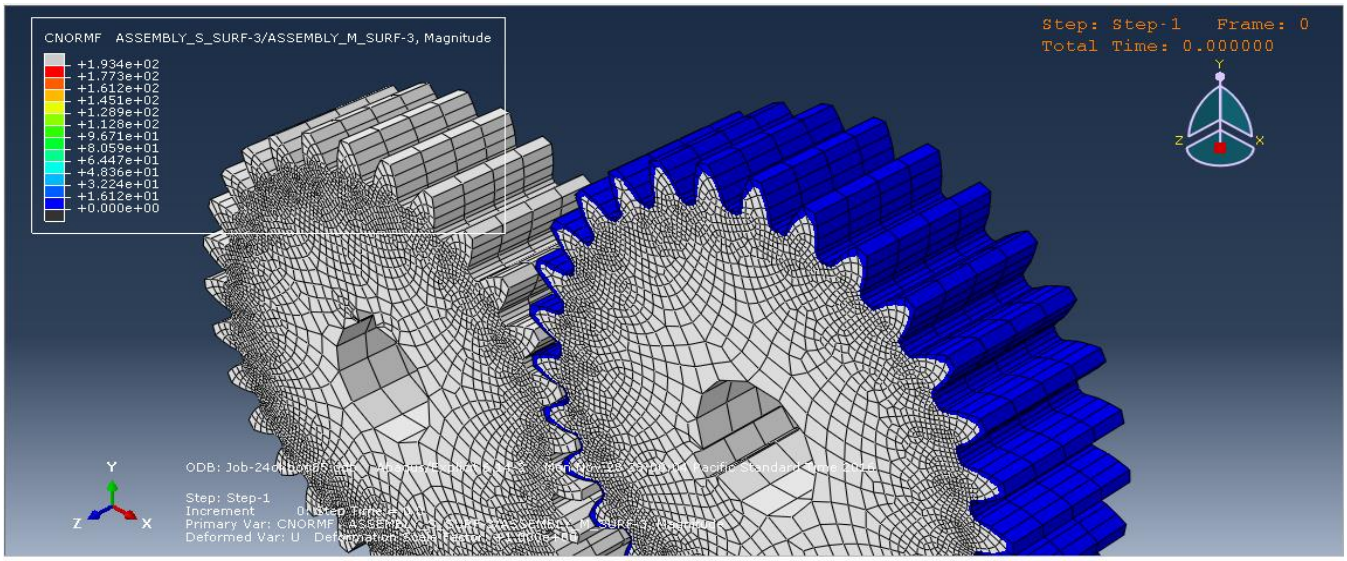

Figure 4. 16Contour Plot for Contact stress

Taking the stress values from the above shown Abaqus/CAE contour plots fatigue life cycles for the root and contact fatigue are calculated according to the previously discussed approach. As it can be seen the maximum bending stress at the root for, 8.5 N.m load is found to be 17.25 MPa. And the maximum contact stress at the root is 16.12 MPa. According to this the life cycle for root fatigue was found to be $1.12*10^7$ cycles and for contact fatigue was found to be $1.64*10^7$ cycles.

The graph below shows the stress(yield) vs number of cycles graph for the material under consideration.

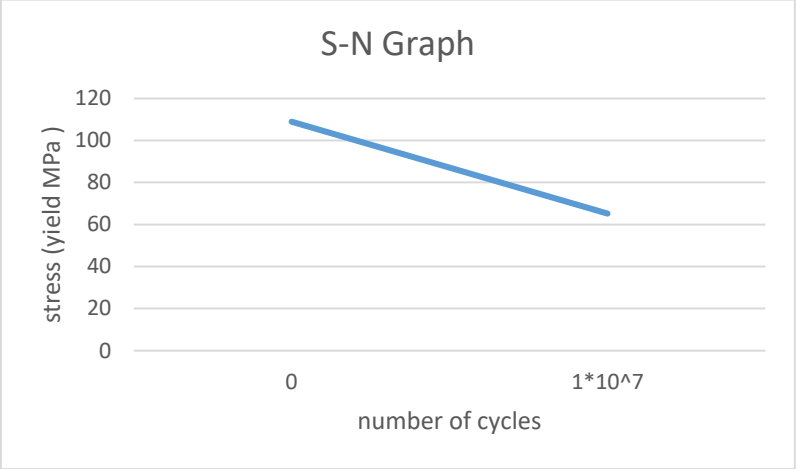

Figure 4. 17 stress vs number of cycles curve for acetal nano-silica composite gear

At the loading condition discussed that is 8.5 N.m and 1000 rpm, the maximum number of life cycle is calculated to be 10^8. According to different literatures the endurance limit of reinforced polymers is found mostly to be in the range of 50-60% of the yield strength, and as it can be seen on the graph above the value is found to be 65.22 MPa.

As it was discussed before the maximum number of cycles for pure acetal gear was found to be 10^6 cycles for the specified loading condition. And from the analysis that was done for nano (SiO_2) reinforced acetal gear it can be seen that the fatigue life of pure acetal gear can be improved by the addition of nano-particles. According to the result obtained, compared to pure acetal gear nano-reinforced acetal gear can run 10 times more cycles under similar loading condition, and the endurance limit is 47% higher than pure acetal.

Chapter five

5. Conclusion and Future work

5.1 Conclusion

As it was discussed in the previous chapter of this work the main goal of this work is to show the advantages of nano reinforced polymer used as a gear material over pure polymer gear. The specific type of polymer used was acetal and comparison was made between the nano(silica) reinforced polymer gear and pure acetal gear for improved wear and thermal resistance as well as fatigue life cycle. After following recommended modeling approaches to find the material property of the composite, Abaqus/CAE 6.14 software was used to find different results to predict the wear and thermal as well as fatigue life of the composite gear. The results were finally compared with the experimental result found for pure acetal gear at the same loading condition, from previously conducted experiment.

As it can be seen from the results obtained from the work done above it can be seen that nano reinforcement of a polymer matrix can greatly impact the overall property of the polymer for only 15.86 grams of mass increased.

- The elastic modulus of the matrix has increased by 265%
- The thermal conductivity has increased by 47%
- Significant amount of change was observed on the wear resistance of the polymer, up to 300%, by the addition of 4.5 volume percentage of nano-silica, which could be due to the high wear resistance of silica.
- The toughness as well as the fatigue life was found to be 10 times better than pure acetal gear.

Considering the application of polymers nano-composite as a gear material is a practical and better option for increasing the application area of polymer gears for different loading or operating conditions. The results show that with the right type of polymer and nano particle combination the problems associated with polymer can be solved and their use as a gear material, especially for medium power transmission can be made possible.

As we compere this gear made of acetal nano-silica composite with a gear made of steel as it can be seen, the material properties like, the elastic modulus is fifty times less than steel, and the thermal conductivity is 100 times less than steel. But the mass of the gear made of acetal nano-silica composite is five times less or lighter than steel. So even though replacing steel as a gear material specially for high power transmission with polymer composites is an area that needs more work, by the encouraging results obtained from this work, more analytical and experimental work must be done, to fully assess the capability of this composites so as to reap the benefits obtained from their unique properties.

5.2 Future Work

Even though this work was done using analytical and modeling approaches which were previously shown with different research works to agree well with experimental results, to fully apply nano silica reinforced polymer gear for power transmission the following future works are recommended.

- Experimental works must be fully conducted using this gear material, based on the promising result obtained here.
- The effect of different sizes and specially shapes of nano-particles must be independently assessed in terms of the main failure modes discussed above.
- The effect of lubrication during running of this gear must also be considered and studied.
- The manufacturing technique of polymer nano-composite gears must be fully studied and the most effective technique to get the best result must be well experimented.

Appendix A

Abaqus contour plots for Von-misses stress and contact pressure

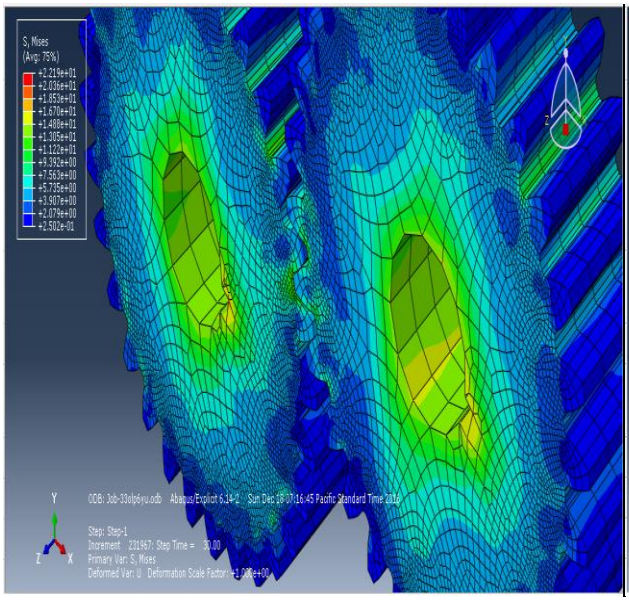

Contour plot of von-misses stress for 6 Nm

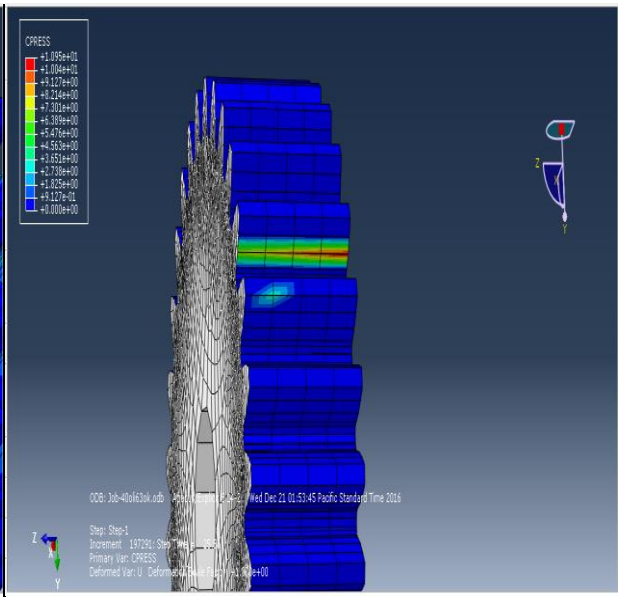

Contour plot of contact pressure for 6 Nm

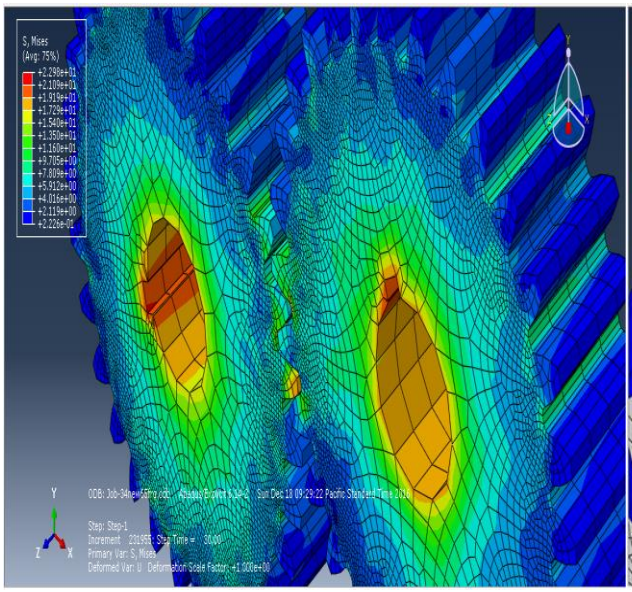

Contour plot of von-misses stress for 6.5 Nm

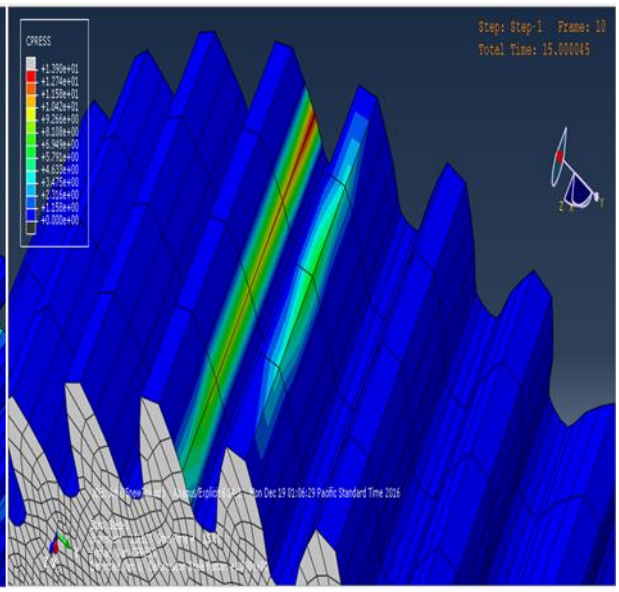

Contour plot of contact pressure for 6.5 Nm

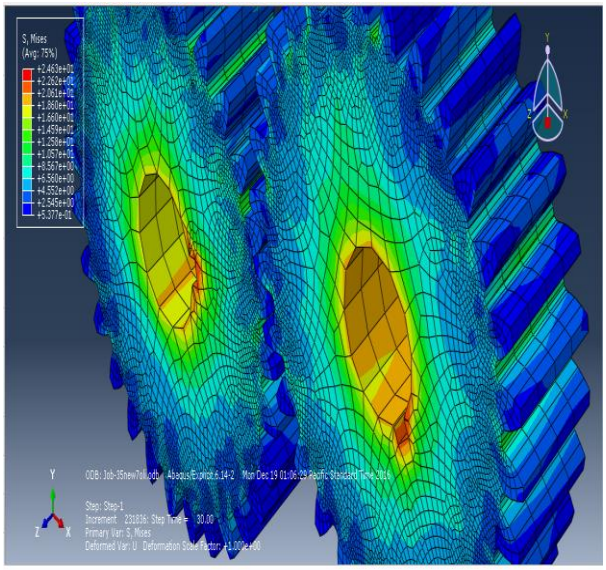

Contour plot of von-misses stress for 7 Nm

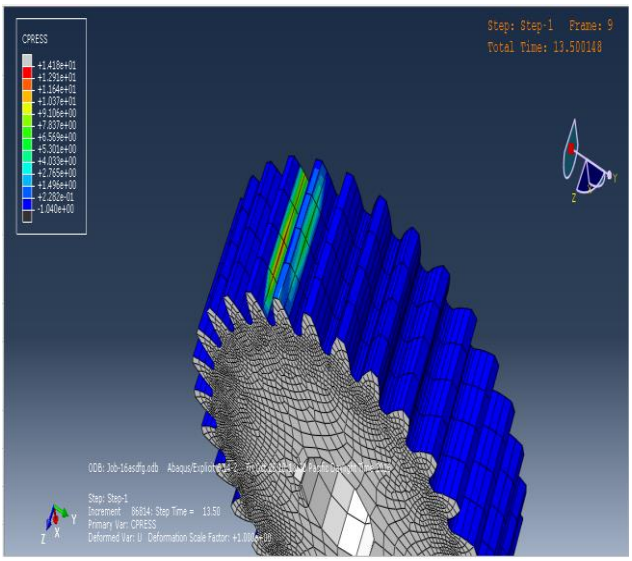

Contour plot of contact pressure for 7 Nm

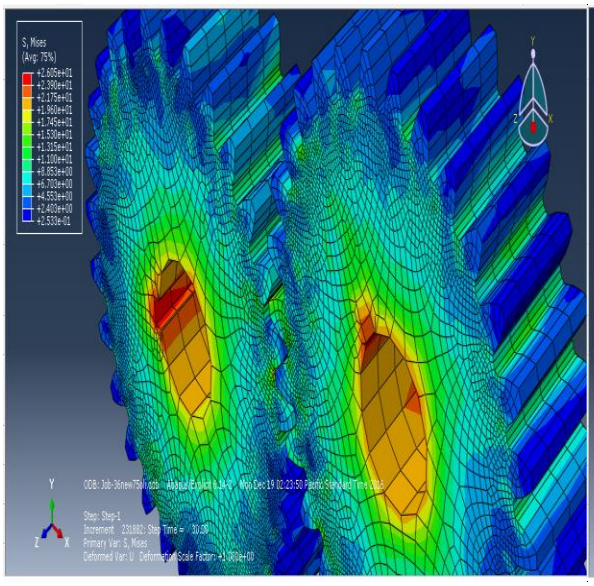

Contour plot of von-misses stress for 7.5 Nm

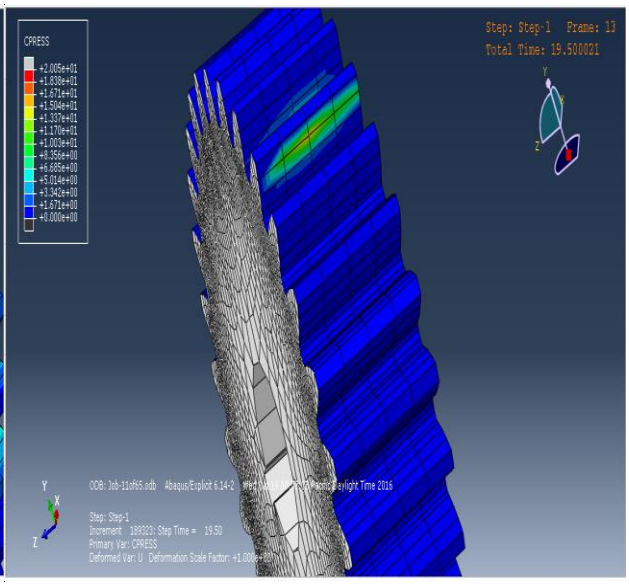

Contour plot of contact pressure for 7 .5 Nm

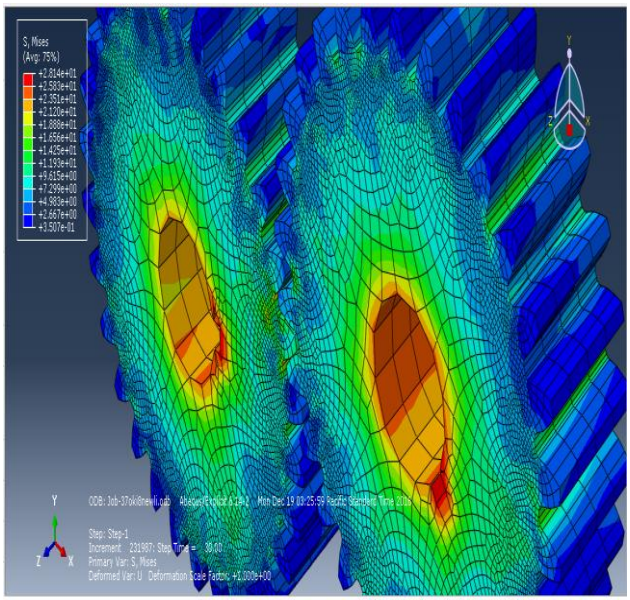

Contour plot of von-misses stress for 8 Nm

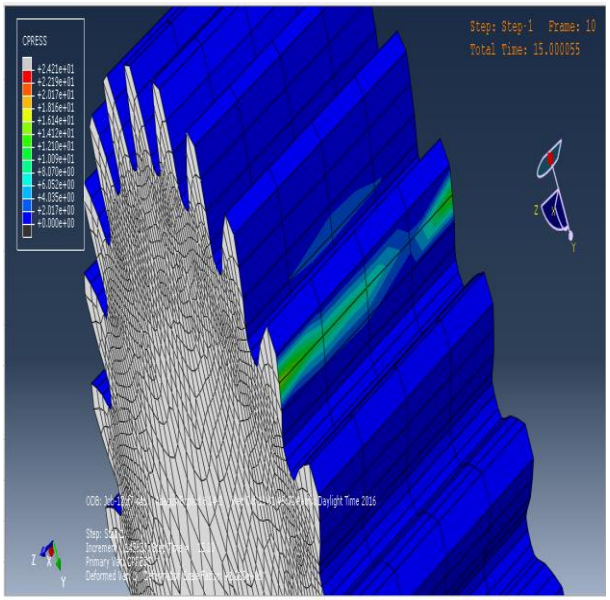

Contour plot of contact pressure for 8 Nm

Appendix B

Mat lab code for the homogenization process

Modeling at nano-level

```
function [Ke,Ge]= nano_model
Gj=25e9;
vj=0.3;
Ej=Gj*2*(1+vj);
Kj=Ej/(3*(1-(2*vj)));
vo=0.3;
Eo=1.4e9;
Go=Eo/(2*(1+vo));
lam=(Eo*vo)/((1+vo)*(1-(2*vo)));
Ko=lam+((2/3)*Go);
a=1e-9;
l=20e-9*(((0.63/0.045)^(1/3))-1);
bg=(1+((20e-9^2)/(2*a*l)));
q=10;
syms rj rk k;
for rj= (2.5e-9:1.5e-9:17.5e-9);
   k=(1:10);
rk=rj+(a.*(1-((k-1)./q)));
Ek=Eo+(Ej-Eo).*((rj+a-rk)/a).^bg;
Kk=Ko+(Kj-Ko).*((rj+a-rk)/a).^bg;
Gk=Go+(Gj-Go).*((rj+a-rk)./a).^bg;
Ck=(rj+(a.*((q-k+1)./q).^3))-(rj+(a.*((q-k)./q).^3))./((rj+a).^3);
Ck1=(rj./(rj+a));
syms W1 W2 Ke Ge;
W1=sum(Ck./(1-(((3*Ke)./((3*Ke)+(4*Ge))).*(1-(Kk./Ke)))));
W2=sum(Ck./(1-(((2*((3*Ke)+(6*Ge)))./(5*((3*Ke)+(4*Ge)))).*(1-(Gk./Ge))))));
[Ke,Ge]=solve(W1-1==0,W2-1==0,Ke,Ge)
end
```

Modeling at micro-model

```
function [Kf,Gf]=mic_model
v=0.3;
Go=1e9;
Eo=Go*(2*(1+v));
lam=(Eo*v)/((1+v)*(1-(2*v)));
Ko=lam+((2/3)*Go);
Csum=0.034;
Co=1-Csum;
ki=1e9;
Ke=1.6257e9;
Ge=-0.1439e9;
ao=((3*Ko)/((3*Ko)+(4*Go)));
ui=23.5e-9;
gam=4.5e-9;
h=1e-9;
for D=(10e-9:37e-9);
yi=D./(2*h);
```

```
Ri=2.7182818284590452353.^-yi.*((yi.^-2)+(yi.^-3))*((yi*3.5000e9*h*yi)-
(3.8462e-10*h*yi));
bo=((6*(Ko+(2*Go))./(5*((3*Ko)+(4*Go)))-((6*ki)./(5*(ki+Go)).*Ri)));
f=((2*pi.*(gam.^2)).^(-1/2).*exp((-((D-ui).^2)./(2*(gam.^2)))));

Kc=((Ko*(1+(((1-Co)*(Ke-Ko))/(Co*ao*(Ke-Ko)+Ko)))));
Gc=((Go.*(1+(((1-Co).*(Ge-Go))./(Co.*bo.*(Ge-Go)+Go)))));
syms Kf Gf D
F=((f./(1-((3*Kf)./((3*Kf)+(4*Gf))).*(1-(Kc/Kf)))));
F1=(f./(1-((2*((3*Kf)+(6*Gf)))./(5*(3*Kf)+(4*Gf))).*(1-(Gc./Gf))));
F3=int(F,D,10e-9,37e-9);
F4=int(F1,D,10e-9,37e-9);

[Kf,Gf]=solve(F3==1,F4==1,Kf,Gf)
end
```

References

[1] K. b. Y. c. S. a. T.J.Hoskins a, "The wearofPEEKinrolling–sliding contact – Simulation ofpolymer," *Wear*, p. 8, 2013.

[2] K. b. Y. c. S. a. T.J.Hoskins a, "The wearof PEEKinrolling–sliding contact – Simulation ofpolymer," *Wear*, p. 8, 2013.

[3] K.Mao, "The wear and termal mechanical behaviour of machine cut polymer gears," *wear*, p. 5, 2015.

[4] C. G. R. G. ⇑. S. Kirupasankar, "Transmission efficiency of polyamide nanocomposite spur gears," *Materials and Design*, p. 8, 2012.

[5] C. G. R. G. S. Kirupasankar, "Transmission efficiency of polyamide nanocomposite spur gears," *Materials and Design*, p. 6, 2011.

[6] J. S. T. P. Olga Konovalova, "Tribological Analysis of the Nano-modified Industrial Polymer," *P r o c e d i a E n g i n e e r i n g*, p. 9, 2014.

[7] Mohammed, "Opportunities and challenges in the use of inorganic," *Progress in Polymer Science*, p. 13, 2013.

[8] c. Li Changa, "Tribological properties of high temperature resistant polymer," *Tribology International 40 (2007) 1170–1178*, p. 9, 2007.

[9] Y. Zare*, "Modeling the Yield Strength of Polymer Nanocomposites Based upon Nano-," *Journal of Colloid and Interface Science*, p. 18, 2016.

[10] P. L. Z. H. K. A. X. X. M. M. W. L. C. H. D. C. K. Mao, "The wear and thermal mechanical contact behaviour of machine cut," *Wear*, p. 6, 2015.

[11] B. Lauke, "On the effect of particle size on fracture toughness of polymer composites," *Composites Science and Technology*, p. 8, 2008.

[12] N. B. L. Parashkevova, "Micropolar-based modeling of size effects on stiffness and yield stress," *Computational Materials Science*, p. 13, 2012.

[13] G. M. a. F. Marino, "Abrasion Resistance of Polymer Nanocomposites – A Review," *Abrasion Resistance of Materials* , p. 19, 2013.

[14] P. n. current, "Polymer nanocomposites: current," *Materials Science and Technology,* p. 15, 2006.

[15] L. Parashkevova, "Micropolar-based modeling of size effects on stiffness and yield stress," *Computational Materials Science,* p. 13, 2012.

[16] Y. Zare, "Estimation of material and interfacial/interphase properties in," *Applied Clay Science,* p. 6, 2015.

[17] I.-Y. J. a. J.-B. Baek, "Nanocomposites Derived from Polymers and Inorganic," *materials* , p. 21, 2010.

[18] J. C. K. H. B. Cotterell, "Fracture mechanisms and fracture toughness in semicrystalline polymer nanocomposites," *Engineering Fracture Mechanics* , p. 26, 2006.

[19] C. S. H. M. Ashfaq Adnan, "A molecular dynamics simulation study to investigate the effect of filler size on elastic properties of polymer nanocomposites," *COMPOSITES,* p. 9, 2006.

[20] J.-Z. Liang, "Reinforcement and quantitative description of inorganic particulate-filled polymer composites," *Composites: Part B,* p. 9, 2013.

[21] J.-Z. Liang, "Reinforcement and quantitative description of inorganic," *Composites: Part B,* p. 9, 2012.

[22] J.-Z. Liang, "Reinforcement and quantitative description of inorganic particulate-filled polymer composites," *Composites: Part B,* p. 9, 2013.

[23] J. C. Z. S. T. T. V. T. Y. Chen, "Mechanical characterization of interfaces in epoxy-clay nanocomposites by molecular simulations," *Polymer,* p. 8, 2012.

[24] M. R. H. H. Abdolhossein Fereidoon, "Fracture analysis of epoxy/SWCNT nanocomposite based on global–local finite element model," *Composites: Part B,* p. 9, 2013.

[25] Y. Zare, "Estimation of material and interfacial/interphase properties in clay/polymer nanocomposites by yield strength data," *Applied Clay Science,* p. 6, 2015.

[26] K. S. M. Z. S. C. M. Quaresimin, "Toughening mechanisms in polymer nanocomposites: From experiments to modelling," *Composites Science and Technology,* p. 53, 2015.

[27] R. Z. H. H. V. H. P. H. A.-B. J. G. de Castro, "Nonmonotonic fracture behavior of polymer nanocomposites," *APPLIED PHYSICS LETTERS*, p. 6, 2015.

[28] S. Z.-R. H. T. T. R. Mohammad Silani, "A semi-concurrent multiscale approach for modeling damage in nanocomposites," *Theoretical and Applied Fracture Mechanics*, p. 9, 2014.

[29] A. E. M. T. K. S. M. A. I. Y. Djebara, "Modeling of the effect of particles size, particles distribution and particles number on mechanical properties of polymer-clay nano-composites: Numerical homogenization versus experimental results," *Composites Part B*, p. 8, 2015.

[30] H. Z. R. P. L. M. J. H.W. Wang, "Nanoreinforced polymer composites: 3D FEM modeling with effective interface concept," *Composites Science and Technology*, p. 9, 2011.

[31] d. H. C. Camargo, "Nanocomposites: Synthesis, Structure,," *material*, p. 12, 10 february 2009.

[32] P. C. W. K. S. E. H. J. Ounaies Z, "Electrical properties," *Composites Science and Technology*, p. 11, 23 february 2003.

[33] G. Z. F. S. W. W. Z. D. Wang C, "Polymers containing fullerene," *Progress in Polymer Science*, p. 13, 15 february 2005.

[34] W. C. H. W. K. Mao, "Polymer gear surface thermal wear and its performance prediction," *Tribology International*, p. 7, 2009.

[35] A. W. K. M. W. Li, "An investigation on the wear behaviour of dissimilar polymer gear engagements," *Wear*, p. 8, 2010.

[36] J. ˇ. T. ˇ. Aljaz ˇ Pogac ˇnik, "An accelerated multilevel test and design procedure for polymer gears," *Materials and Design*, p. 13, 2014.

[37] K. Mao, "A new approach for polymer composite gear design," *Wear*, p. 10, 2006.

[38] "An investigation on the wear behaviour of dissimilar polymer gear engagements," p. 8, 2010.

[39] K. Mao, "A numerical method for polymer composite gear flash temperature prediction," *Wear*, p. 9, 2006.

[40] K. Mao, "A new approach for polymer composite gear design," *Wear*, p. 10, 2006.

[41] D. K. L. T. F. E. Alencar Bravo, "Life and damage mode modeling applied to plastic gears," *Engineering Failure Analysis,* p. 21, 2015.

[42] W. C. H. D. K. Mao, "Friction and wear behaviour of acetal and nylon gears," *Wear,* p. 7, 2008.

[43] "Polymergearsurfacethermalwearanditsperformanceprediction," *TribologyInternational,* p. 7, 2009.

[44] A. M. Díez-Pascual, "High-performance nanocomposites based on," *Progress in Materials Science,* p. 85, 2012.

[45] L. P. ⇑, "Micropolar-based modeling of size effects on stiffness and yield stress," *Computational Materials Science,* p. 13, 2012.

[46] M. Conradi, "NANOSILICA-REINFORCED POLYMER COMPOSITES," *MTAEC9,* p. 9, 2013.

[47] V. K. T. B. L. M. a. A. P. J. Karger-Kocsis, "On the toughness of thermoplastic polymer nanocomposites as assessed by the essential work of fracture (EWF) approach," *Composite Interfaces,,* p. 10, 2013.

[48] A. ˇ. P. ˇ. a, "An accelerated multilevel test and design procedure for polymer gears," *Materials and Design,* p. 13, 2013.

[49] A. W. R. W. K. M. W. Li a, "An investigation on the wear behaviour of dissimilar polymer gear engagements," *Wear,* p. 8, 2010.